GPS constraints on continental deformation in the Africa-Arabia-Eurasia continental collision zone and implications for the dynamics of plate interactions

Robert Reilinger,[1] Simon McClusky,[1] Philippe Vernant,[1] Shawn Lawrence,[1,2] Semih Ergintav,[3] Rahsan Cakmak,[3] Haluk Ozener,[4] Fakhraddin Kadirov,[5] Ibrahim Guliev,[5] Ruben Stepanyan,[6] Merab Nadariya,[7] Galaktion Hahubia,[7] Salah Mahmoud,[8] K. Sakr,[8] Abdullah ArRajehi,[9] Demitris Paradissis,[10] A. Al-Aydrus,[11] Mikhail Prilepin,[12] Tamara Guseva,[12] Emre Evren,[13,14] Andriy Dmitrotsa,[15] S. V. Filikov,[15] Francisco Gomez,[16] Riad Al-Ghazzi,[17] and Gebran Karam[18]

Received 15 September 2005; revised 13 January 2006; accepted 31 January 2006; published 31 May 2006.

[1] The GPS-derived velocity field (1988–2005) for the zone of interaction of the Arabian, African (Nubian, Somalian), and Eurasian plates indicates counterclockwise rotation of a broad area of the Earth's surface including the Arabian plate, adjacent parts of the Zagros and central Iran, Turkey, and the Aegean/Peloponnesus relative to Eurasia at rates in the range of 20–30 mm/yr. This relatively rapid motion occurs within the framework of the slow-moving (~5 mm/yr relative motions) Eurasian, Nubian, and Somalian plates. The circulatory pattern of motion increases in rate toward the Hellenic trench system. We develop an elastic block model to constrain present-day plate motions (relative Euler vectors), regional deformation within the interplate zone, and slip rates for major faults. Substantial areas of continental lithosphere within the region of plate interaction show coherent motion with internal deformations below ~1–2 mm/yr, including central and eastern Anatolia (Turkey), the southwestern Aegean/Peloponnesus, the Lesser Caucasus, and Central Iran. Geodetic slip rates for major block-bounding structures are mostly comparable to geologic rates estimated for the most recent geological period (~3–5 Myr). We find that the convergence of Arabia with Eurasia is accommodated in large part by lateral transport within the interior part of the collision zone and lithospheric shortening along the Caucasus and Zagros mountain belts around the periphery of the collision zone. In addition, we find that the principal boundary between the westerly moving Anatolian plate and Arabia (East Anatolian fault) is presently characterized by pure left-lateral strike slip with no fault-normal convergence. This implies that ''extrusion'' is not presently inducing westward motion of Anatolia. On the basis of the observed kinematics, we hypothesize that deformation in the Africa-Arabia-Eurasia collision zone is driven in large part by rollback of the subducting African lithosphere beneath the Hellenic and Cyprus trenches aided by slab pull on the southeastern side of the subducting Arabian plate along the Makran subduction zone. We

[1]Department of Earth, Atmospheric, and Planetary Sciences, Massachusetts Institute of Technology, Cambridge, Massachusetts, USA.
[2]Now at University Navstar Consortium (UNAVCO), Boulder, Colorado, USA.
[3]Turkish National Science Foundation, Marmara Research Center, Earth and Marine Sciences Research Institute, Gebze, Turkey.
[4]Kandilli Observatory and Earthquake Research Institute, Bogazici University, Istanbul, Turkey.
[5]Geology Institute, National Academy of Sciences, Baku, Azerbaijan.
[6]National Survey for Seismic Protection, Yerevan, Armenia.
[7]Joint Stock Company ''Airgeodetic'', Tbilisi, Georgia.
[8]National Research Institute of Astronomy and Geophysics, Helwan, Cairo, Egypt.
[9]King Abdulaziz City for Science and Technology, Riyadh, Kingdom of Saudi Arabia.
[10]Higher Geodesy Laboratory, National Technical University, Athens, Greece.
[11]Faculty of Science, Sana'a University, Yemen.
[12]Universal Institute of Physics of the Earth, Moscow, Russia.
[13]Eurasian Institute of Earth Sciences, Istanbul Technical University, Istanbul, Turkey.
[14]Now at Geophysics Research Group, University of Ulster, Coleraine, County Derry, Northern Ireland.
[15]Crimea Radio Astronomical Observatory, Simiez, Crimea, Ukraine.
[16]Department of Geological Sciences, University of Missouri–Columbia, Columbia, Missouri, USA.
[17]Higher Institute of Applied Science and Technology, Damascus, Syria.
[18]Department of Civil Engineering, Lebanese American University, Jbeil, Lebanon.

0148-0227/06/2005JB004051$09.00

further suggest that the separation of Arabia from Africa is a response to plate motions induced by active subduction.

Citation: Reilinger, R., et al. (2006), GPS constraints on continental deformation in the Africa-Arabia-Eurasia continental collision zone and implications for the dynamics of plate interactions, *J. Geophys. Res.*, *111*, B05411, doi:10.1029/2005JB004051.

1. Introduction

[2] The eastern Mediterranean, Asia Minor, the Middle East, and northeast Africa is a zone of complex tectonics associated with the interaction of four of the Earth's major lithospheric plates, Arabia, Nubia, Somalia, and Eurasia (Figures 1a and 1b). *McKenzie* [1970, 1972] and *McKenzie et al.* [1970] provided a first-order, plate tectonic description of the region, recognizing active continental collision in eastern Turkey, the Caucasus, and the Zagros; lateral transport of Anatolia (Turkey) toward the west accommodated by the North and East Anatolian faults; subduction of African oceanic lithosphere (i.e., Neotethys) along the Hellenic and Cyprus trenches; extension in the Aegean and western Turkey; crustal spreading along the East African Rift system; and ocean rifting along the Red Sea and Gulf of Aden. In regard to general principles that control continental deformation, *McKenzie* [1972] further suggested that large areas of continental lithosphere appear to be aseismic and not deforming at present, that plate tectonic concepts provide a useful description of continental deformation, and that continental lithosphere tends to move laterally out of zones of continental collision to avoid excessive crustal thickening. Subsequent studies have added important refinements to this tectonic characterization [e.g., *Jackson and McKenzie*, 1984, 1988], including the partitioning of crustal deformation in the eastern Turkey/Caucasus continental collision zone [*Jackson*, 1992], the importance of subduction and slab retreat along the Hellenic trench as a dynamic mechanism for extension in the Aegean and western Turkey [e.g., *Le Pichon and Angelier*, 1979; *Sonder and England*, 1989; *Royden*, 1993], and the influence of slab detachment on regional tectonics [e.g., *Spakman*, 1991; *Wortel and Spakman*, 2000; *Şengör et al.*, 2003].

[3] Understanding the dynamics of plate motions and interactions (i.e., the primary forces acting on the plates) and the rheology of the continental lithosphere are among the most fundamental questions in active tectonics [e.g., *Tapponnier et al.*, 2001; *Thatcher*, 2003; *Wright et al.*, 2004; *Conrad and Lithgow-Bertelloni*, 2004]. While it was recognized early in the development of plate tectonics that plate boundaries in continental areas are substantially wider than those in the oceans [e.g., *Isacks et al.*, 1968; *Molnar and Tapponier*, 1975], the underlying causes of this different behavior and the most appropriate way to describe continental deformation (i.e., continuum vs. microplate or block behavior) remain under debate. For the eastern Mediterranean this debate has centered on the interaction of the Arabian plate with Eurasia and the apparent ''extrusion'' of Anatolia toward the west from the zone of most intense convergence. One school of thought [e.g., *McKenzie*, 1978; *England and McKenzie*, 1983] considers the continental lithosphere to be weak and models it as a thin viscous sheet. They conclude that gravitational potential energy associated with the thickened continental crust within the collision zone drives lateral motion out of the area of maximum convergence. An alternate model [e.g., *Tapponier et al.*, 1982; *Şengör et al.*, 1985; *Philip et al.*, 1989] considers the continental lithosphere to be strong and attributes lateral motions from the zone of maximum compression to forces acting on the edges of the plates. In the case of Arabia/Eurasia collision, this amounts to Anatolia being pushed along its SE edge by the impinging Arabia plate.

[4] Since the mid-1980s, the Global Positioning System (GPS) has provided earth scientists a new opportunity to estimate directly present-day surface motions and deformations [e.g., *Hager et al.*, 1991]. In the eastern Mediterranean, prior GPS studies have helped quantify large-scale plate motions [e.g., *Sella et al.*, 2002; *McClusky et al.*, 2003; *Fernandez et al.*, 2003, 2004], regional deformation in the zone of plate interaction [e.g., *Le Pichon et al.*, 1995; *Reilinger et al.*, 1997; *Davies et al.*, 1997; *Clarke et al.*, 1998; *McClusky et al.*, 2000; *Kahle et al.*, 2000; *Goldsworthy et al.*, 2002; *Vernant et al.*, 2004a, 2004b; *Nyst and Thatcher*, 2004; *Mahmoud et al.*, 2005], and deformations associated with the earthquake cycle [e.g., *Hubert-Ferrari et al.*, 2000; *Reilinger et al.*, 2000; *Delouis et al.*, 2002; *Hearn et al.*, 2002a; *Ergintav et al.*, 2002; *Meade et al.*, 2002]. The kinematic information provided by GPS is in turn providing new constraints on the rheology and dynamics of the continental lithosphere [e.g., *Meijer and Wortel*, 1997; *Lundgren et al.*, 1998; *Wortel and Spakman*, 2000; *Mantovani et al.*, 2001; *Jiménez-Munt and Sabadini*, 2002; *Hearn et al.*, 2002b; *Provost et al.*, 2003; *Flerit et al.*, 2004].

[5] In this paper we present a new GPS-derived velocity field including data from 1988 to 2005, updating the results presented by *McClusky et al.* [2000]. We formally incorporate new, published GPS data from the Iran-French GPS Project [*Vernant et al.*, 2004a, 2004b] and in east Africa [*Bendick et al.*, 2005], and new observations on the Arabian plate to determine an internally consistent velocity field extending west-east from the Adriatic Sea to the Iran-Afghanistan border, and north-south from the Russian platform to the East African rift. We use the extensive velocity data to constrain an elastic block model [*Meade and Hager*, 2005] developed on the basis of available geologic, seismic, and other geophysical data. Finally, we consider the implications of the new velocity data and kinematic model results for the dynamics of continental deformation in the eastern Mediterranean, Arabia, and northeast Africa region.

2. GPS Data and Analysis

[6] Table S1 in the auxiliary material lists details of the GPS observations and the horizontal velocity components derived from measurements made between 1988 and 2005.[1]

[1] Auxiliary material is available at ftp://ftp.agu.org/apend/jb/2005jb004051.

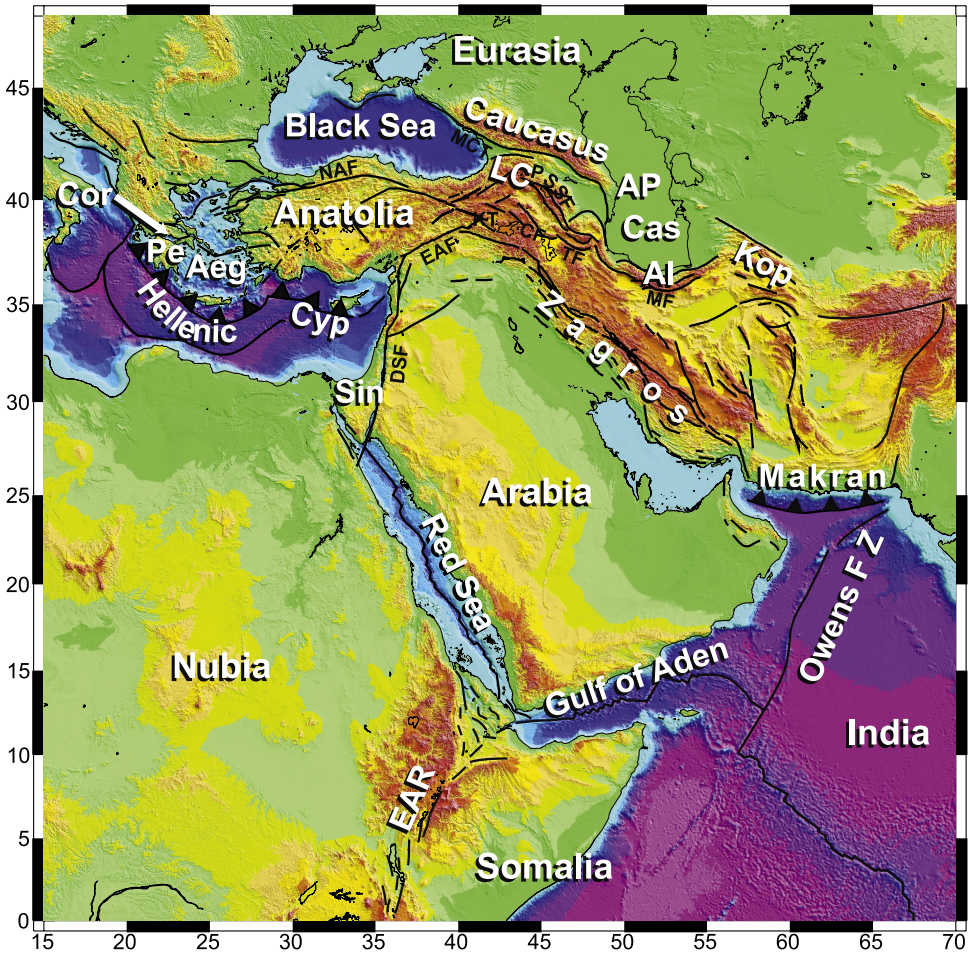

Figure 1a. Simplified topographic/bathymetric (SRTM30 PLUS; http://topex.ucsd.edu/WWW_html/srtm30_plus.html) and tectonic map of the study area, including the zone of interaction of the Nubian, Somalian, Arabian, and Eurasian plates. Abbreviations are North Anatolian fault (NAF), East Anatolian fault (EAF), Dead Sea fault (DSF), Mosha fault (MF), Pembak-Sevan-Sunik fault (PSSF), Tabriz fault (TF), Chalderan fault (CF), Gulf of Corinth (Cor), Peloponnesus (Pe), Aegean (Aeg), Lesser Caucasus (LC), Cyprus trench (Cyp), Karliova Triple junction (KT), Sinai (Sin), Caspian Sea (Cas), Main Caucasus Thrust (MCT), East African rift (EAR), Kopet Dag (Kop), Apsheron Peninsula (AP), Alborz Mountains (Al).

In Figures 2 and 3 the velocities are plotted in a Eurasia-fixed reference frame (1σ error ellipses are shown in Figure 2 for clarity; Figure 3 shows 95% confidence ellipses). GPS velocities are determined for 440 stations, 337 measured with survey mode GPS (SGPS) and 103 are continuous stations (CGPS) in the study area (i.e., not including global stations used in the analysis). As indicated in Table S1, velocities are determined for different time spans, although the large majority of SGPS measurement campaigns were conducted between August and October in order to minimize annual systematic errors.

[7] We analyze the GPS data using the GAMIT/GLOBK software [*King and Bock*, 2004; *Herring*, 2004] in a two-step approach [*Dong et al.*, 1998]. In the first step, we use GPS phase observations from each day to estimate station coordinates, the zenith delay of the atmosphere at each station, and orbital and Earth orientation parameters (EOP). In the second step we use the loosely constrained estimates of station coordinates, orbits, and EOP and their covariances from each day, aggregated by survey, as quasi-observations in a Kalman filter to estimate a consistent set of coordinates and velocities. We provide orbital control and tie the regional measurements to an external global reference frame by including in the regional analysis data from 5 to 10 continuously operating IGS stations for each day. The regional quasi-observations are then combined with quasi-observations from an analysis of phase data from over 250 stations performed by the Scripps Orbital and Permanent Array Center (SOPAC) at University of California, San Diego [*Bock et al.*, 1997].

[8] Before estimating velocities in the second step of our analysis, we examine all of the position time series for outliers and offsets or "jumps." To account for correlated errors in the time series, we calculate a unique noise model for each station. The algorithm used to model the data noise spectrum assumes that each time series can be adequately modeled using a first-order Gauss Markov (FOGM) process noise described in equation (1) [*Gelb*, 1974]. The FOGM noise model is estimated from individual stations time series

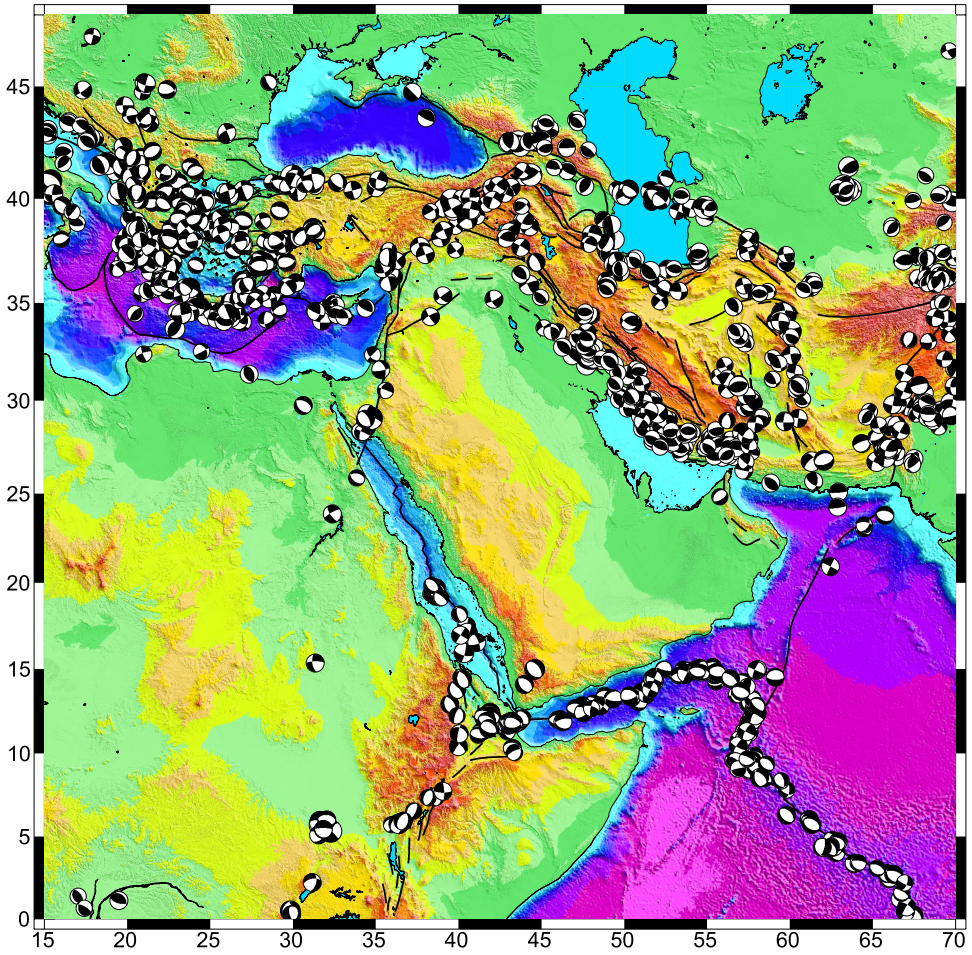

Figure 1b. Focal mechanisms for earthquakes in the study area (lower hemisphere projections) from Harvard catalog, 1976 to January 2005. Base map is as in Figure 1a.

by averaging the residuals over increasingly longer intervals. The averaging intervals range from a minimum of 7 days to a maximum of 1/10th of the total time series span (days) increasing sequentially by 7-day increments. For each interval we compute the χ^2 per degree of freedom (χ^2/dof). As expected for nonwhite noise spectra the χ^2/dof values increase with increasing averaging time for nearly all times series. (For a site with a white process noise, the χ^2/dof value would remain constant.) The interval-averaged χ^2/dof values are then fit to the FOGM model where a correlation time and long-term variance are estimated. This estimated FOGM model is then used to predict the site velocity uncertainty based on the time span of the time series. Since GLOBK uses a random walk (RW) process noise model (which is a special case of the FOGM model where the correlation time $1/\beta$ is infinite), we then calculate the RW process noise model that would predict the same velocity uncertainty as the FOGM model at the time series span interval. These RW process noise values are then used in the forward run of the GLOBK Kalman filter (using the same data as was used in the time series) to estimate site velocities and "realistic" uncertainties. Since this method of estimating site-dependent process noise is only applicable to continuous time series (as we need to be able to average over a range of time series sampling intervals), the RW process noise applied to SGPS sites in the Mediterranean region was obtained by taking the average of the RW noise estimates for CGPS sites in the region (1.3 mm/$\sqrt{}$yr).

$$\varphi_{xx}(\tau) = \sigma^2 e^{-\beta|\tau|} \quad (1)$$

where $\varphi_{xx}(\tau)$ is the first-order Gauss-Markov autocorrelation function, σ^2 is the long-term variance, and $1/\beta$ is the correlation time.

[9] Unless indicated otherwise, uncertainties quoted in the text, Tables 1, 2, S1, and S3, and Figure 2 are 1σ estimates while those shown in Figures 1 and 3–14 are 95% confidence ellipses.

[10] The reference frame for our velocity estimates is defined in the second step, in which we apply generalized constraints [*Dong et al.*, 1998] while estimating a six-parameter transformation (six components of the rate of change of translation and rotation). Specifically we define the reference frame by minimizing the horizontal velocities of 49 global IGS core stations with respect to the IGS00 realization of ITRF2000 NNR frame (ITRF2000I) [*Ray et al.*, 2004]. The WRMS fit of our solution to the ITRF2000I reference frame is 0.6 mm/yr. Finally we rotate our ITRF2000I velocity field into a Eurasian fixed frame. Using 32 stations located on the Eurasian plate, the Eurasia-

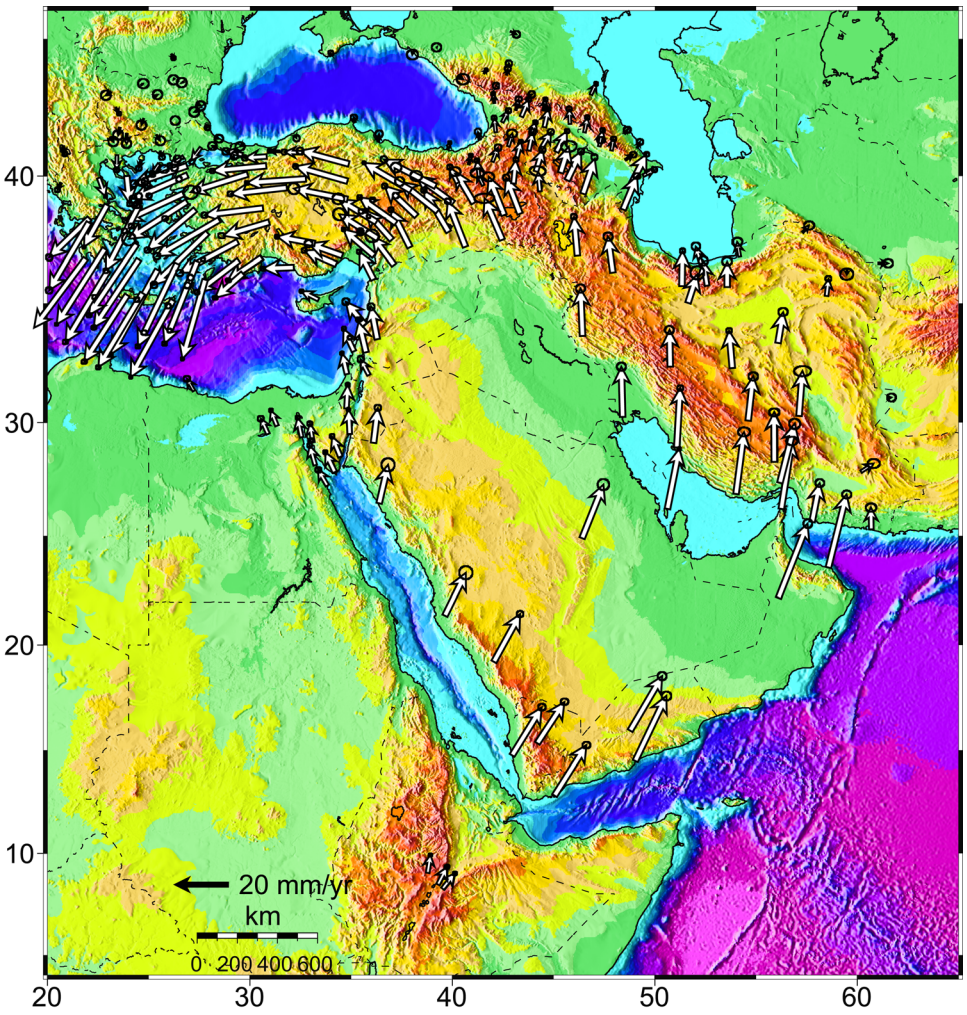

Figure 2. Map showing decimated GPS velocities relative to Eurasia determined in this study. For clarity, we plot 1σ velocity uncertainties (see Table S1 for a complete tabulation of the velocities determined in this study). Topography is as in Figure 1a.

ITRF2000I Euler vector is estimated in a simultaneous least squares solution, using the velocity solution and its associated full variance covariance matrix. The WRMS fit of the 32 sites to a nondeforming Eurasian plate is 0.5 mm/yr. Velocities in this realization of the Eurasian fixed reference frame and their associated 1σ standard deviations are given in Table S1.

3. Principal Features of the GPS Velocity Field

[11] A striking aspect of the velocity map shown in Figure 2 is the rapid motion (~20–30 mm/yr) characterizing the Arabian Peninsula, adjacent parts of Iran and the Caucasus, and the Anatolia/Aegean region within the framework of the large and slowly moving (relative to each other ~5 mm/yr) Eurasian, Nubian, and Somalian plates. These rapid motions are dominated by large-scale counterclockwise rotation that encompasses Arabia, Anatolia, and the Aegean region. The entire continental region south of the North Anatolian fault (NAF), and its E-SE extension into central and southern Iran, an area of roughly 7×10^6 km^2 (~5% of the Earth's continental surface), is involved in this circulatory pattern. Furthermore, the rate of motion defining this counterclockwise circulation appears to increase toward the Hellenic trench system. Following an arc from the northern Arabian plate to the Hellenic trench (Figure 3), velocities in the Eurasia reference frame increase in magnitude from 17.8 ± 1.1 mm/yr (KIZI) on the northernmost Arabian plate in SE Turkey to 20.6 ± 0.8 mm/yr in eastern and central Turkey (SINC, ANKT), to 24.6 ± 1.0 mm/yr in western Turkey (YAYA), and to 31.1 ± 0.9 mm/yr in the central and southern Aegean (KYNS). In addition, the Sinai/Levant block and the Nubian Plate show trenchward motion (Figure 3). While we consider the implications of the velocity field for regional dynamics in a subsequent section of this paper, the apparently coherent pattern of surface motion encompassing an area with dimensions >3000 km within a region of large, slowly moving plates suggests a deep-seated dynamic source. Furthermore, the predominance of trenchward motion, and the increasing rates of motion toward the eastern Mediterranean trench system appear to us as strong evidence that the principal forces driving Anatolia, and perhaps the majority of deformation in the eastern Mediterranean, arise from processes directly

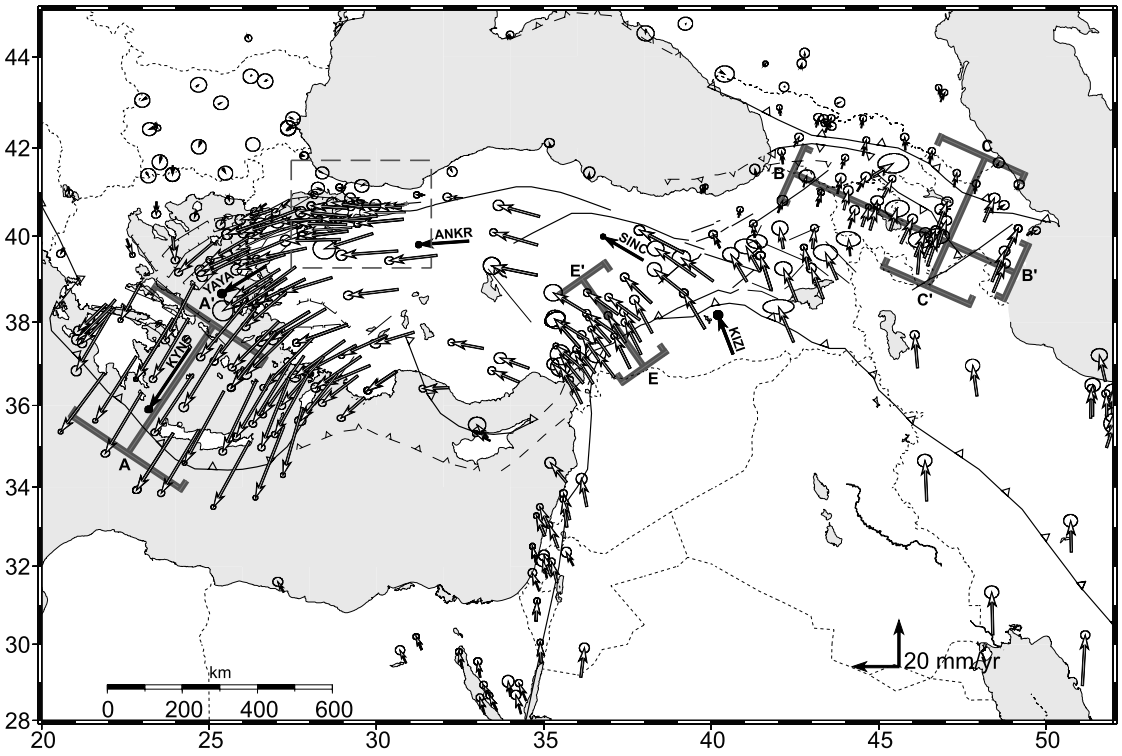

Figure 3. Map showing GPS velocities with respect to Eurasia and 95% confidence ellipses for the NW part of the study area. Locations and widths (brackets) of velocity profiles crossing the Aegean (A–A′) (Figures 4a and 4b), along and across strike of the Greater Caucasus (B-B′, and C-C′, respectively) (Figures 4c–4f), and crossing the EAF (E–E′) (Figures 6a and 6b) are also shown. The dashed box shows the area covered in Figure 5a. Dark velocity vectors with four-character IDs are referred to in the text and illustrate the progressive increase in rate from the north Arabian platform to the Hellenic Trench.

related to active subduction of the African lithosphere along the Hellenic and Cyprus trenches, a mechanism that has been under discussion since the advent of modern plate tectonics [e.g., *Elsasser*, 1971; *Wortel and Spakman*, 2000].

[12] The Aegean region is characterized by very uniform (magnitude and orientation) GPS velocities (Figure 3). This is well illustrated by Figures 4a and 4b that show the profile-parallel and profile-normal velocity components for a profile oriented in the direction of Aegean-Eurasia relative motion (Figure 3, profile A-A′) for a broad area ($\sim$1.4 $\times$ 10^5 km^2) of the Aegean and Peloponnesus. The profiles indicate SW translation at about 30.5 mm/yr roughly normal to the west Hellenic trench with <2 mm/yr variation.

[13] The new velocity determinations in the Lesser Caucasus show a clear tendency to be directed more easterly (i.e., turning from NW or north to NE) progressing from south to north for regions east of about 42°E. This longitude marks the northernmost promontory of the Arabian ''indenter''. Divergence of motions north of the Arabian promontory appears consistent with the notion of Arabia displacing continental material laterally as it impinges on the Eurasian plate [e.g., *Şengör et al.*, 1985].

[14] Another feature apparent in the improved Caucasus velocity field is the tendency for motion rates to increase from west to east along strike of the Main Caucasus Thrust (i.e., $\sim$120° azimuth). Also, there is little change in the magnitude of velocity estimates across much of the Lesser Caucasus along transects perpendicular to the Caucasus range. This is illustrated in the velocity profiles oriented along strike (Figure 3, B-B′), and crossing (C-C′) the Caucasus range (Figures 4c, 4d, 4e, and 4f, respectively). Given the low level of seismic activity within the Lesser Caucasus (Figure 1b, see also Figure 7), we interpret these observations to imply block-like, counterclockwise rotation of the Lesser Caucasus resulting in increased convergence from west to east along the Main Caucasus Thrust (MCT). This behavior is not unlike that of Anatolia and Aegean in that all three regions appear to be moving with little internal deformation.

[15] As noted earlier by *McClusky et al.* [2000], there is a tendency for continental lithosphere to move around the Black Sea. This motion is accommodated by the striking velocity change across the NAF and the tendency for motions to turn toward the east around the eastern side of the Black Sea (Figure 3). *McClusky et al.* [2000] suggested that the oceanic lithosphere underlying the Black Sea is fundamentally stronger than the continental lithosphere to the south and hence represents a ''backstop'' resisting deformation and deflecting the impinging continental lithosphere.

4. Block Model

[16] *McClusky et al.* [2000] showed that the GPS-derived velocity field in the eastern Mediterranean is well described kinematically by a system of undeforming regions separated by spatially confined zones of deformation, as was sug-

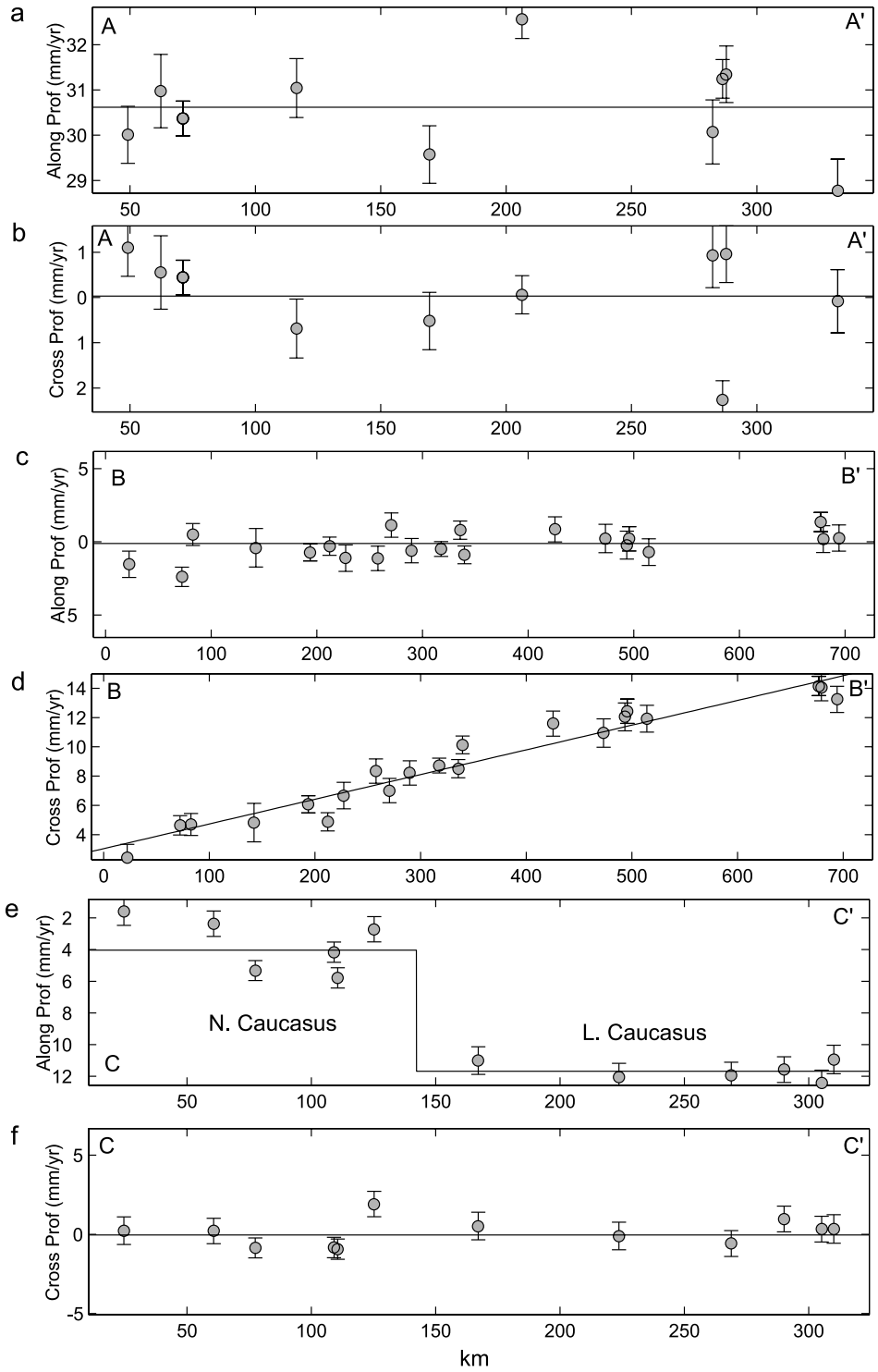

Figure 4. GPS velocities with respect to Eurasia with 1σ uncertainties plotted versus distance along profiles shown in Figure 3. The widths of the profiles are indicated by brackets in Figure 3. (a) Aegean profile (A-A′) showing profile-parallel velocities (component of velocity in direction of Aegean motion with respect to Eurasia). (b) Aegean profile (A-A′) showing profile-normal velocity components. (c) Caucasus profile (B-B′; oriented parallel to the strike of the Main Caucasus Thrust) showing profile-parallel velocity components. (d) Caucasus profile (B-B′) showing profile-normal velocity components and illustrating progressive increase in the rate of convergence from NW to SE along strike of the Caucasus. (e) Caucasus profile (C-C′; oriented normal to the strike of the Main Caucasus Thrust) showing profile-parallel velocity components and illustrating the concentration of convergence along the MCT and coherent motion of the Lesser Caucasus (N. Caucasus, north Caucasus, L Caucasus, Lesser Caucasus). (f) Caucasus profile (C-C′) showing profile-normal velocity components.

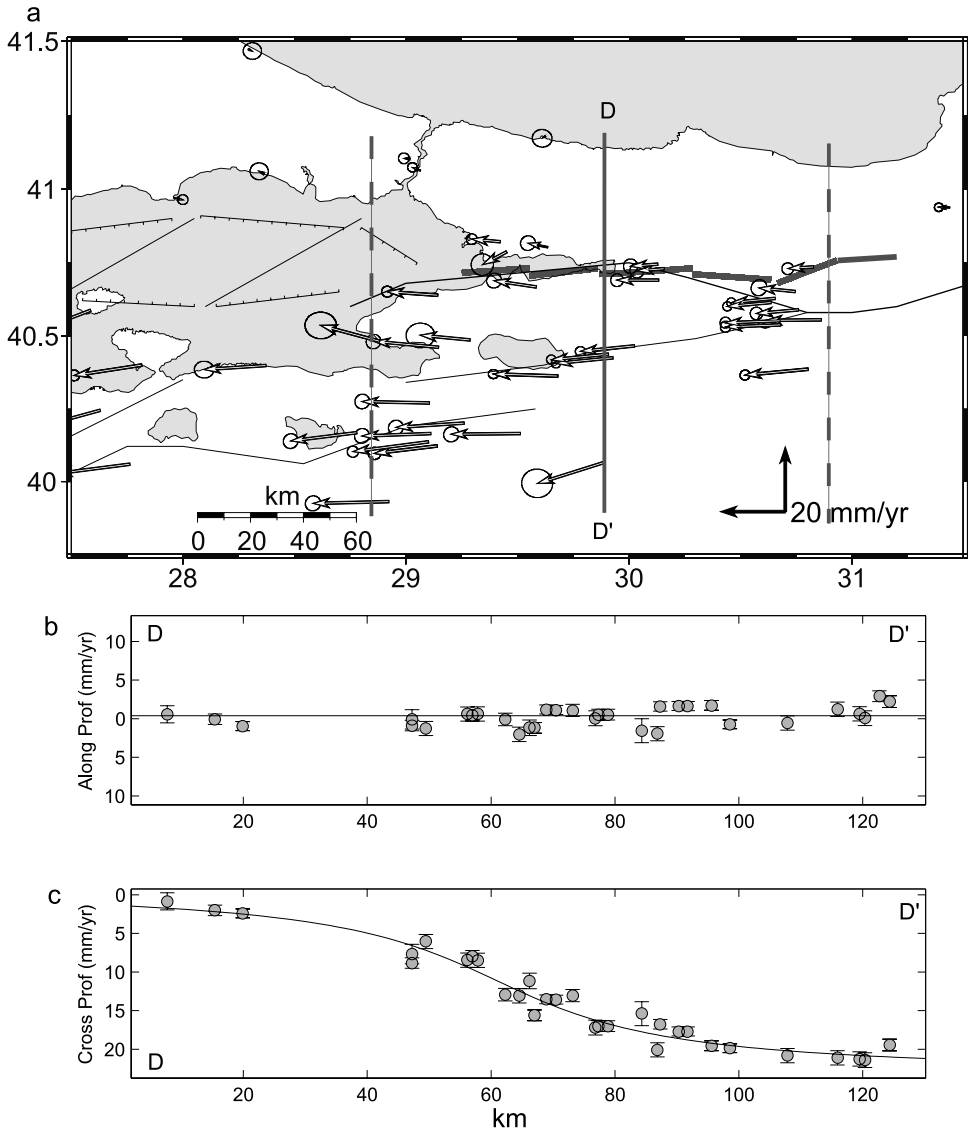

Figure 5. (a) Map of GPS velocities relative to Eurasia and 95% confidence ellipses in the Marmara region (see Figure 3 for location) for the pre-Izmit earthquake period (1988–1999 preearthquake) and location of the trans-NAF profile. Dashed lines show the width of the profile which includes the segment of the NAF that broke in the M = 7.4, 1999, Izmit, Turkey, earthquake (heavy, segmented line). (b) Profile-parallel velocity components and 1σ uncertainties plotted versus distance along profile. (c) Profile-normal velocity components and 1σ uncertainties plotted versus distance along profile. The curve shows the theoretical pattern of strain accumulation for an infinitely long, vertical strike-slip fault locked to a depth of 21 km.

gested earlier [e.g., *McKenzie*, 1970] on the basis of the distribution of earthquakes [also see *Reilinger and McClusky*, 2001; *Nyst and Thatcher*, 2004]. Similarly, *Vernant et al.* [2004a] and *Mahmoud et al.* [2005] emphasize the apparent coherent motions of central Iran and the Sinai, respectively. The updated velocity field presented here supports this view, indicating that to first order, large regions of continental lithosphere move coherently (e.g., east/central Anatolia, Aegean, Lesser Caucasus). In addition, where sufficient GPS coverage is available in the near field of active faults, deformation is fit well by the arctangent function characteristic of elastic strain accumulation [*Okada*, 1985]. This behavior is illustrated in Figure 5, which shows velocity profiles crossing the western NAF. The profiles show the pattern of right-lateral strain accumulation for the segment of the NAF that broke in the 1999, M_w = 7.4, Izmit, Turkey, earthquake. GPS site velocities are derived from pre-1999 earthquake observations (i.e., not including coseismic or postseismic deformation [*Reilinger et al.*, 2000; *Ergintav et al.*, 2002]). The simple, two-dimensional (2-D) elastic half-space model shown in Figure 5 indicates a locking depth of ~21 km. Considering that we don't include the southern branch of the NAF that will tend to broaden the deformation and hence imply a greater locking depth, the geodetically determined locking depth is roughly consistent with the depths of the 1999 main

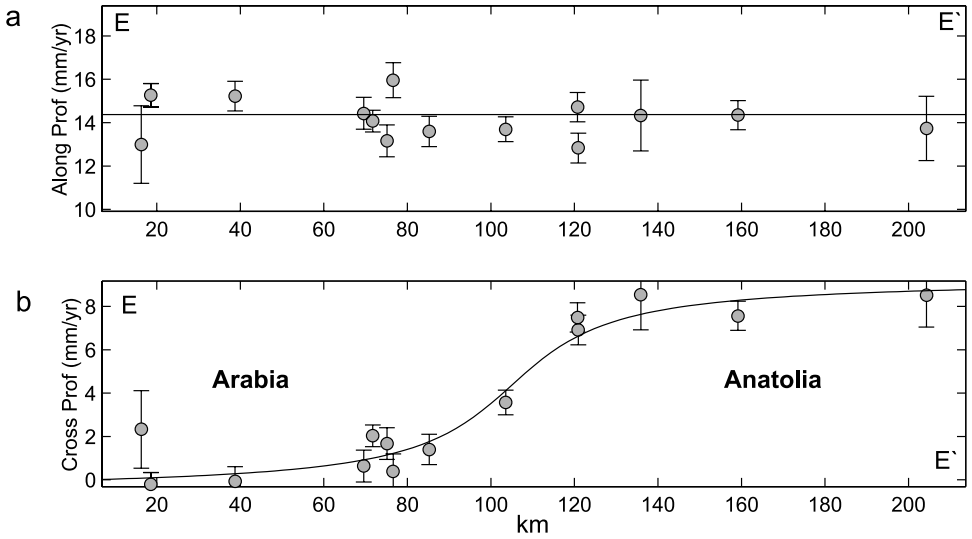

Figure 6. (a) East Anatolian fault velocity profile showing profile-parallel velocities and 1σ uncertainties relative to Eurasia (E-E′; see Figure 3 for profile location and width). (b) East Anatolian fault velocity profile (E-E′; Figure 3) showing profile-normal velocities. The curve is the theoretical strain accumulation for a vertical, infinitely long strike-slip fault locked to a depth of 18 km.

event (∼13 km) and subsequent larger aftershocks (∼8–17 km) [*Ozalaybey et al.*, 2002]. Similar results are indicated in Figures 6a and 6b for the EAF (∼18 km locking depth) and by *Wdowinski et al.* [2004] and *Mahmoud et al.* [2005] for the Dead Sea fault.

[17] These observations lead us to investigate kinematic block models that include the effect of elastic strain accumulation on block boundaries [e.g., *Meade et al.*, 2002; *McCaffrey*, 2002; *Meade and Hager*, 2005]. Our preferred model is shown in Figure 7 (see Table S2 for a compilation of faults used in the model). Block boundaries are prescribed and have been determined from mapped faults, seismicity, and historic earthquakes. Many of the major faults in the eastern Mediterranean are well defined (historic earthquakes, mapped coseismic surface offsets, seismicity, and geologic field studies). These faults are shown as light lines in Figure 7. Less clearly defined block boundaries are shown as gray lines. The model includes block rotations on a sphere with elastic strain accumulation on block-bounding faults following the formulation of *Okada* [1985]. The model allows no permanent deformation of the blocks or slip on "unconnected" fault segments (i.e., all faults used in the model must be associated with a block boundary). Relative block motions (relative Euler vectors, Table 1) are solved for by minimizing the GPS residual motions (Figures 8a–8d) within the blocks in a least squares sense. Modeled faults are vertical except for thrusts which are assigned a 30° dip (shown with triangles in Figure 7). Most faults are assigned a 15 km locking depth, measured vertically from the surface for vertical and dipping faults. The NAF in the Marmara Sea, the DSF, and the Gulf of Corinth fault are locked to 10, 12, and 2 km, respectively, based on prior studies (NAF by *Meade et al.* [2002] and DSF by *Mahmoud et al.* [2005]), and the sharp velocity contrast across the Gulf of Corinth. Fault slip rates, shown in Figures 9a–9d (see Table S2 for a complete compilation), are determined by decomposing relative block motions on block boundaries into fault parallel (strike slip, positive left-lateral) and fault-normal motions (normal and thrust, positive compression).

[18] WRMS residuals for each plate/block are given in Table 1. As indicated in Table 1 and Figure 8, the block model provides a reasonable fit to the GPS velocity field, accounting for the large majority of observed motions. About 63% of the observed velocities in the region are fit within their 95% confidence ellipses, while about 95% differ by less than 2 mm/yr. While more complex models would provide better fits to the data, the relatively simple model we use captures the main kinematics in the zone of plate interaction.

[19] For most faults in the model, the GPS coverage is not sufficiently dense near the faults to provide good constraints on fault locking depths. This adds an additional uncertainty to model slip rates because there is a trade-off between locking depth and slip rate [*Meade and Hager*, 2005] (slip rate increases with locking depth). This trade-off occurs because GPS velocities near a locked fault will have smaller velocities than those within the block far from the fault due to the effects of strain accumulation. Since the smaller velocities near the fault are not accounted for by strain accumulation for models with shallow locking depth, the model tends to give slower plate velocities for more shallowly locked faults, and hence lower slip rates. This is illustrated in Figure 10 which shows a plot of local χ^2 (a measure of goodness of fit to the model [*Meade and Hager*, 2005]) and estimated slip rate versus fault locking depth for a section of the NAF, one of the better constrained faults in the model (Figures 3 and 5). The local χ^2 is determined using the GPS stations shown in the inset of Figure 10. The minimum χ^2 (i.e., best model fit) is for locking depths in the range 14–25 km, quite reasonable given the depths of earthquakes. This adds an additional uncertainty of about ±1 mm/yr for this fault. This is among the highest slip rate variations as a function of fault locking depth for any boundary fault (model slip rates on block boundaries with few stations near the fault are insensitive to variations in

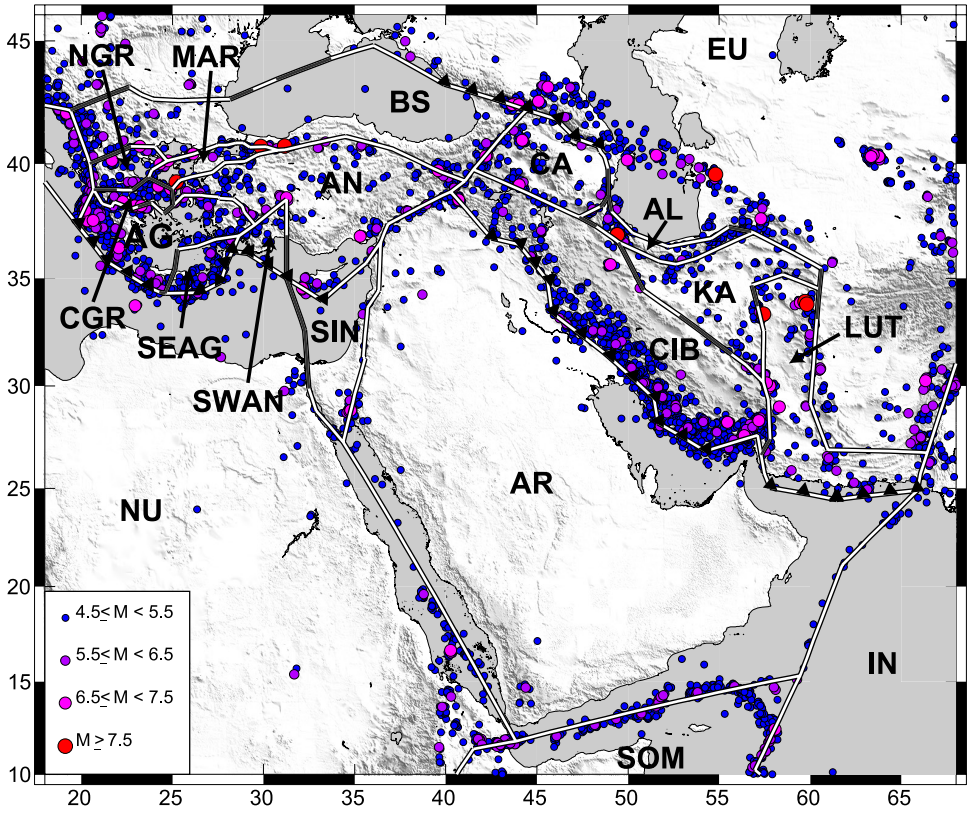

Figure 7. Map showing our preferred block model consisting of 19 plates/blocks and $M > 4.5$ earthquakes above 35 km depth (National Earthquake Information Center catalog; 1973 to January 2005). Details of the block boundaries are given in Table S2. White lines show well-defined boundaries that follow known, active faults. Black lines show less well defined boundaries. Lines with triangles are thrust faults dipping 30°. All other boundaries are vertical. See text for discussion of the model. Abbreviations are Nubian (NU), Somalian (SOM), Arabian (AR), Eurasian (EU), Anatolian (AN), Aegean (AG), Lut (LUT), central Iran block (CIB), Kavir (KA), Alborz (AL), Caucasus (CA), Black Sea (BS), Sinai (SIN), southwest Anatolian (SWAN), southeast Aegean (SEAG), central Greece (CGR), northern Greece (NGR), Marmara (MAR), India (IN).

assumed locking depth). Because the effect is small, and it is impossible to rigorously determine the variation in fault locking depths for our model, we do not attempt to include uncertainties in locking depths in our slip rate estimates.

[20] Fault slip rates also depend on the angle between the direction of relative motion between adjacent blocks and the local strike of the fault at that location. The fault-normal rate varies as the sine of this angle and the fault parallel rate as the cosine. This is well illustrated by the variation in slip rates along the Dead Sea fault at the Lebanon restraining bend. Comparisons between the geodetically determined slip rates indicated by our model and local geologic estimates along specific fault segments need to take this into account. For example, for the EAF (slip rate ~10 mm/yr), a variation of ±5° results in a change in fault-normal slip rate of ~0.7 mm/yr, and ~1.7 mm/yr for the NAF (slip rate ~25 mm/yr). There is no resolvable effect on the fault parallel rate for either fault. The block boundaries we use in our model are not meant to represent details of the faults but rather the general character of the zone of interplate deformation. Detailed comparisons to specific fault segments will require more careful consideration of the local orientation of the fault segment in relation to the relative motion of adjacent blocks.

[21] The uncertainties on fault slip rates reported in this study (text and Tables 2 and S2) are formal uncertainties reflecting only the uncertainties in the relative Euler vectors. They do not include uncertainties in model parameters, including fault locking depth, fault location, and fault dip. Accordingly, the reported uncertainties underestimate the true uncertainty in slip rate. While we can't provide rigorous uncertainties, our experience indicates that model fault slip rates in western Turkey, and central Greece can vary substantially between different models (±3 mm/yr) because of the large number of small blocks and uncertainty about fault geometry. On the other hand, most model faults further east where fault geometry is constrained better (including the NAF, DSF, EAF, Zagros, and Main Caucasus Thrust (MCT)) have variations of ±2 mm/yr or less (e.g., compare Figure 9b with Figures 11b and 13).

[22] Clearly, our regional block model is highly idealized. Complex deformational structures such as the Zagros Fold and Thrust belt are modeled as a single fault. This idealized fault will necessarily accommodate both strike-slip and dip-slip motions. In fact, deformation is likely partitioned between different structures [e.g., *Talebian and Jackson*, 2002]. Even relatively simple faults such as the EAF and NAF are more complex than indicated by the model [e.g.,

Table 1. Euler Vectors Relative to Eurasia and 1σ Uncertainties for the Block Model Determined in This and Prior Studies[a]

Plates[b]	Longitude, °E	σ	Latitude, °N	σ	Rate, deg/Myr	σ	Correction	WRMS, mm/yr	Number of Sites	References[c]
NU-EU	−23.9	1.5	−2.3	1.1	0.059	0.001	0.0130	1.29	39	ts
NU-EU	−21.8	4.3	−0.95	4.8	0.06	0.005				mc1
NU-EU	−20.01	4.5	−18.23	9.1	0.062	0.005	−0.52			se
NU-EU	−20.6	0.8	21.0	6.0	0.12	0.015	−0.51			nu
AR-EU	18.4	1.0	28.4	0.9	0.428	0.009	0.029	1.57	33	ts
AR-EU	18.4	2.5	27.4	1.0	0.40	0.04				mc1
AR-EU	19.7	4.1	25.6	2.1	0.5	0.1				mc
AR-EU	22.87	2.1	26.22	1.2	0.427	0.029	0.31			se
AR-EU	19.5	1.4	27.9	0.5	0.41	0.1				ve
AR-EU	13.7	5.0	24.6	2.3	0.5	0.05	−0.63			nu
AR-NU	25.2	0.7	31.5	0.6	0.393	0.005	0.061			ts
AR-NU	25.7	2.3	30.5	1.0	0.37	0.04				mc1
AR-NU	23.0	2.7	31.5	1.2	0.40	0.05				chu
AR-NU	24.0		32.2		0.376					jg
AR-NU	23.7		32.59		0.418					je
AR-SOM	27.4	1.0	20.3	0.6	0.455	0.008	−0.031			ts
AR-SOM	26		25		0.450					jg
AR-SOM	23.39	4.5	25.24	2.4	0.423	0.05	−0.88			je
AR-SOM	24		24		0.41					gd
AR-SIN	28.4	3.7	32.8	3.4	0.370	0.027	0.226			ts
AR-SIN	30.00	5.72	28.71	3.86	0.2114	0.1584	−0.688			wd
AR-SIN	22.6		32.8		0.283					jg
AN-EU	32.1	0.7	30.8	0.8	1.231	0.023	0.174	2.55	56	ts
AN-EU	32.6	0.4	30.8	0.8	1.2	0.1				mc
AN-EU	14.6		34		0.64					jm
AN-EU	14.6		34		0.78					t
AN-EU	31		35.5		0.83	0.1				w
AN-EU	30		34		0.44					lp
AN-EU	32.73		32.03		1.72					lp1
AG-EU	52.3	2.9	15.9	2.7	0.563	0.028	0.154	2.44	28	ts
AG-EU	161.77	3.61	−45.91	0.05	−0.52	0.03				nt
MAR-EU	28.4	2.1	35.1	2.4	2.370	0.106	0.258	2.47	30	ts
MAR-EU	28.68		36.1		2.50					lp2
SEAG-EU	16.8	2.9	−37.9	4.0	2.531	0.177	−0.291	1.76	5	ts
SWAN-EU	32.2	3.3	34.5	3.3	3.774	0.238	0.282	2.41	9	ts
BS-EU	31.4	2.1	43.3	2.1	0.231	0.010	0.267	1.97	57	ts
SIN-EU	−19.1	22.0	1.8	25.4	0.088	0.041	−0.012	1.61	20	ts
SIN-EU	16.62	15.45	23.14	9.49	0.2242	0.1477	0.996			wd
SIN-NU	−9.6	0.038	9.7	44.1	0.030	0.021	0.0			ts
SIN-NU	26.34	8.28	31.04	1.96	0.2029	0.1543	0.535			wd
SIN-NU	28.1		30.3		0.093					jg
CA-EU	37.8	3.8	42.1	3.6	0.84	0.06	−0.058	1.97	27	ts
NGR-EU	19.1	0.8	38.6	0.3	−1.511	0.317	0.0	2.07	3	ts
CGR-EU	19.8	0.2	39.9	0.1	−4.266	0.210	0.0	0.97	7	ts
CGR-EU	19.99	0.06	39.78	0.02	−4.34	0.10				nt
KA-EU	81.5	14.9	29.4	4.9	−0.225	0.124	0.0	1.42	8	ts
LUT-EU	83.2	13.9	26.1	4.8	−0.152	0.079	0.0	2.45	2	ts
AL-EU	57.9	3.0	36.6	0.6	−1.299	0.790	0.0	1.95	4	ts
CIB-EU	4.2	0.1	18.9	4.9	0.207	0.020	0.018	1.93	19	ts
CIB-EU	65.8		27.5		0.56					jm
CIB-EU	0.98	1.2	23.15	13.2	0.189	0.1				ve
SOM-EU	74.4	5.4	−29.1	3.8	−0.093	0.011	0.0	1.80	6	ts
SOM-NU	35.5	4.2	−27.0	2.4	−0.104	0.007	0.099			ts
SOM-NU	36.2	4.8	−27.3	6.7	−0.089	0.004	0.90			cg
SOM-NU	19.76		−55.735		−0.054					je
SOM-NU	24.02	3.3	−35.49	4.7	−0.085	0.005	−0.28			se
SOM-NU	36.97	4.9	−54.76	9.4	−0.069	0.009	−0.28			fe
SOM-NU	33.0		−6.9		−0.091					jg
IN-EU	27.1	2.4	30.3	1.0	0.441	0.01	−0.637	0.88	4	ts
IN-EU	11.62	14.4	28.56	1.13	0.357	0.033	−0.221			se
IN-EU	17.7	8.65	24.4	2.44	0.51	0.05	−0.660			nu
IN-AR	110.9	6.7	17.7	4.9	0.060	0.01	0.326			ts
IN-AR	61.83	17.9	10.5	10.4	0.099	0.037	0.037			se
IN-AR	92	22.21	3	13.9	0.03	0.04	−0.99			gd
IN-AR	91.50	21.41	3.0	13.51	0.03	0.04	−0.978			nu

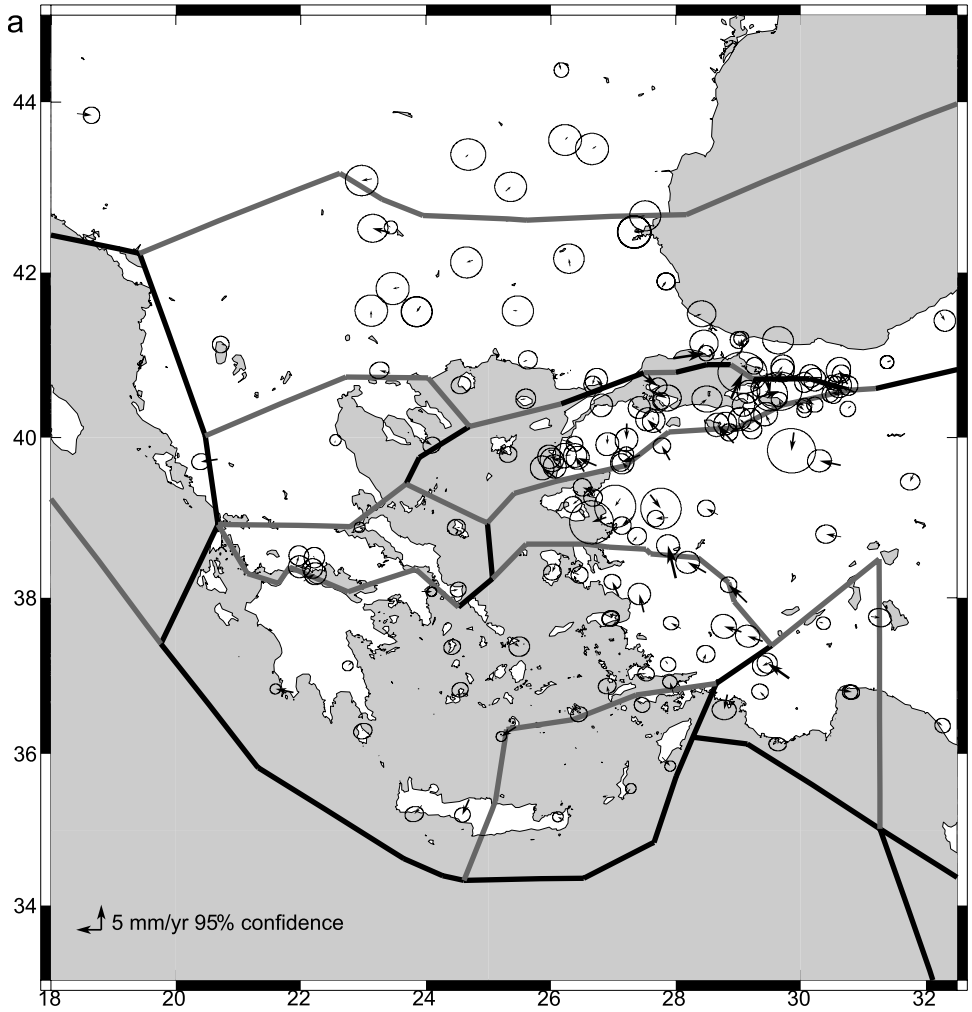

Figure 8. Maps showing residual velocities (observed minus modeled) and 95% confidence ellipses for the block model shown in Figure 7 and described in the text. Light block boundaries show fault-normal opening and dark show fault-normal closing. Residual velocities are listed in Table S2.

Şengör et al., 2004; *Westaway*, 2004]. In the Caspian Sea region, current data are not able to distinguish between models that include, or not, a southern Caspian block (i.e., with a boundary following the seismicity across the central Caspian to the Kopet Dag, Figure 7). We do not include this block since it would be virtually unconstrained. A southward turn of the MCT near the Caspian Sea seems necessary, however, given the low rate of motion for the station south of the Apsheron Peninsula (Figure 3). Similarly, the western boundary of the Sinai block is not well constrained by geophysical observations or by the GPS results [*Mahmoud et al.*, 2005], and the Lut (LUT) and northern Greece (NGR) blocks are poorly constrained by the GPS data (Figures 8a and 8c). The Euler vectors for these blocks are preliminary at best. In spite of these limitations, we believe the relatively simple model we use (19 blocks) is appropriate for our regional study given available geodetic constraints, and that it captures the primary structures controlling regional deformation, the main focus of this paper. In addition, we suggest that block models provide a well-understood, physical basis to investigate possible deformation associated with unmodeled faults and/or possible anelastic deformation of blocks. Many studies demonstrate that strain accumulation measured on the Earth's surface

Notes to Table 1:

[a]The number of GPS sites and WRMS residuals for each block in our model are also given. Selected relative Euler vectors for other block pairs are given for comparison to other published results.

[b]Plate abbreviations are EU, Eurasia; NU, Nubia; AR, Arabia; AN, Anatolia; AG, Aegean; MAR, Marmara; SEAG, SE Aegean; SWAN, SW Anatolia; BS, Black Sea; SIN, Sinai; CA, Caucasus; NGR, northern Greece; CGR, central Greece; KA, Dasht-e-Kavir region; LUT, Lut block; SOM, Somalia; AL, Alborz and Kopet Dagh mountains; CIB, central Iranian block; IN, India.

[c]References are ts, this study; chu, *Chu and Gordon* [1998]; cg, *Chu and Gordon* [1999]; fe, *Fernandez et al.* [2004]; gd, *Gordon and DeMets* [1989]; jm, *Jackson and McKenzie* [1984]; je, *Jestin et al.* [1994]; jg, *Joffe and Garfunkel* [1987]; lp, *Le Pichon and Angelier* [1979]; lp1, *Le Pichon et al.* [1995]; lp2, *Le Pichon et al.* [2003]; mc, *McClusky et al.* [2000]; mc1, *McClusky et al.* [2003]; nt, *Nyst and Thatcher* [2004]; nu, NUVEL1-A [*DeMets et al.*, 1994]; se, *Sella et al.* [2002]; t, *Taymaz et al.* [1991]; ve, *Vernant et al.* [2004a]; wd, *Wdowinski et al.* [2004]; w, *Westaway* [1994].

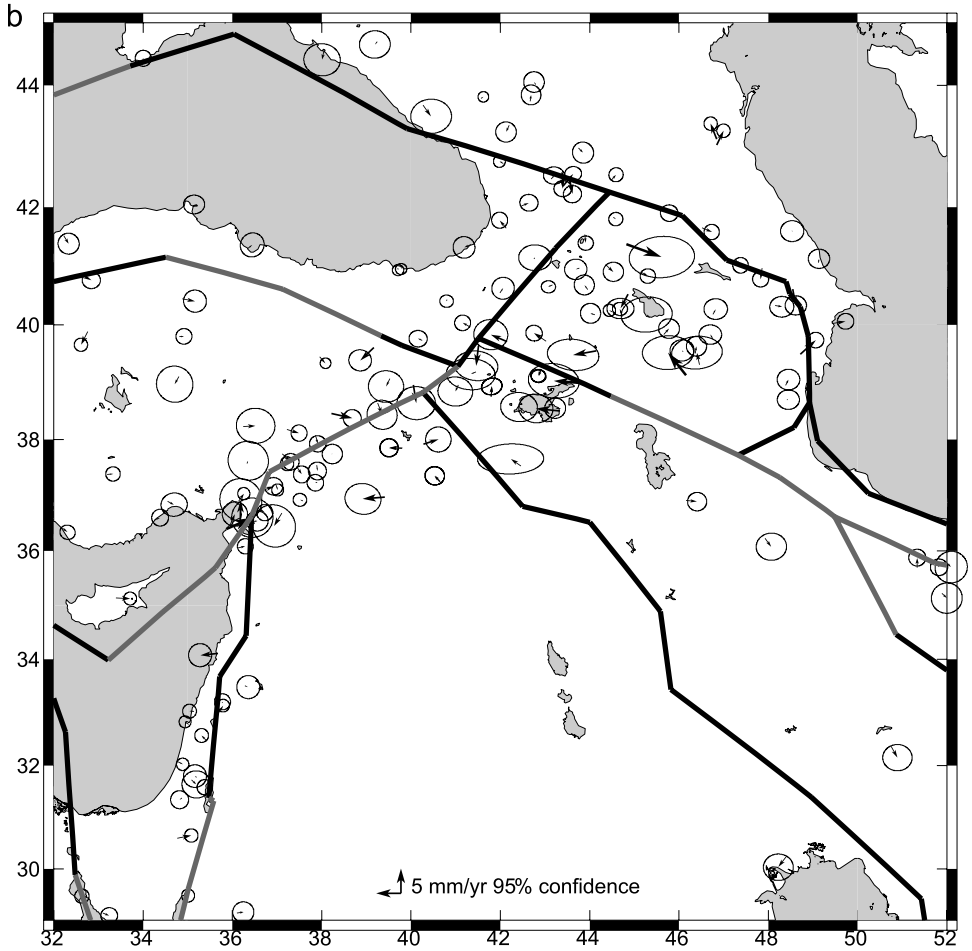

Figure 8. (continued)

during the interseismic period is well characterized by models that consider faults as buried, deep dislocations in an elastic half-space with the upper part of the fault locked to depths of typically 10–25 km (e.g., Figures 5 and 6) [*Okada*, 1985]. While such models may not be an accurate representation of the physics of faulting or the rheology of the lithosphere, they provide a good representation of fault-related surface deformation [e.g., *Savage*, 1990]. As such, we suggest that the elastic block model effectively removes those motions that are associated with strain accumulation on block bounding faults, allowing identification of off-fault deformation associated with either unmodeled faults or permanent strain within the blocks.

[23] While the block model provides a good fit to the observations overall, a number of areas show significant residual motions that likely reflect inadequacies of the model. Residual motions in western Turkey are large, reaching 7 mm/yr and indicating unmodeled N-S extension. Internal deformation of this area is also indicated by seismicity (Figures 1b and 7) and local active fault studies [*Westaway*, 1994; *Bozkurt*, 2003]. Certainly, more detailed modeling is warranted in this area, although beyond the scope of this regional study. In addition, there is evidence of a small component of trench-parallel extension (~2 mm/yr) along the leading edge of both the SW and SE Aegean blocks. This extension is consistent with mapped normal faults [*Armijo et al.*, 1992] and extensional earthquake focal mechanisms with nodal planes striking normal to the trench (Figure 1b). In the Lesser Caucasus there is marginally significant evidence for right-lateral strike-slip deformation along the Pembak-Sevan-Sunik Fault (PSSF), Armenia (possible source of the 1988, M = 6.9, Spitak earthquake [*Dorbath and Cisternas*, 1997]). Figures 11a and 11b shows the results of a block model including two blocks in the eastern Turkey Plateau–Lesser Caucasus. The boundary follows the PSSF and connects with the complex structures near the SW Caspian Sea. The model results in only a slight reduction in GPS residuals, but suggests a right-lateral slip rate for the PSSF of ~3.5 mm/yr, consistent within uncertainties with results from paleoseismic studies [*Trifonov et al.*, 1994; *Philip et al.*, 2001] (Table 2).

5. Discussion

5.1. Relative Euler Vectors

[24] Euler vectors for the Nubian, Arabian, and Anatolian plates relative to Eurasia are generally consistent with those reported in prior geodetic studies (Table 1). Similarly, the geodetic and geologic Euler vectors for Arabia-Nubia, Somalia-Nubia, and Arabia-Somalia relative motion are in good agreement using the most recent geologic results. The discrepancy between our geodetic Euler vector and the

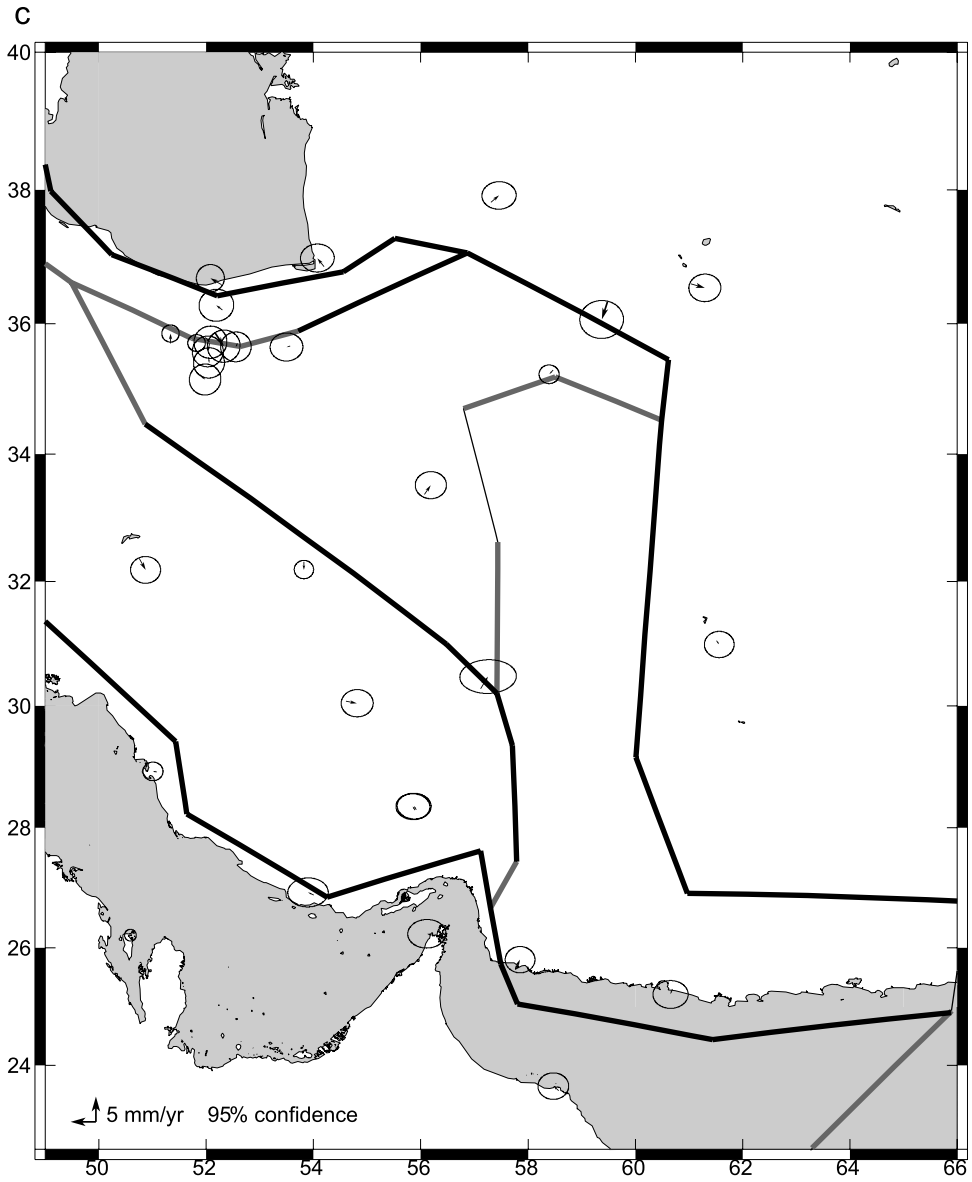

Figure 8. (continued)

geologic Euler vector for Africa-Eurasia relative motion reported for the NUVEL1-A model [*DeMets et al.*, 1990, 1994] is not surprising since the NUVEL model considered Nubia and Somalia as a single plate because of the lack of data to distinguish individual plate motions. Recently, *McQuarrie et al.* [2003] reevaluated Africa (Nubia)–Eurasia relative motion from 67.7 Ma to present from updated seafloor magnetic anomalies in the North Atlantic. They report a post-10 Ma average rate of 7.5 ± 4 mm/yr at 38°N, 48°E for Africa (Nubia) plate motion with respect to Eurasia which compares to 6.4 ± 1 mm/yr from the Nubia-Eurasia GPS Euler vector. In this same study, *McQuarrie et al.* [2003] report a rate of 20 ± 4 mm/yr (38°N, 48°E) for Arabia-Eurasia relative motion (incorporating Red Sea spreading) that also agrees well with the present-day rate determined from the Arabia-Eurasia GPS Euler vector (21 ± 1 mm/yr). While interpretations differ (*Calais et al.* [2003] suggest temporal variations in Nubia-Eurasia plate motion), we take this general agreement as support for the hypothesis that broad-scale plate motions indicated by GPS for Arabia, Nubia, Somalia, and Eurasia accurately reflect plate motions during the recent geologic period (∼5 Myr).

[25] Geologic estimates of relative motions are not available for most of the smaller blocks within the zone of interaction of the Nubian, Arabian and Eurasian plates. However, it is possible to compare the GPS fault slip rate estimates to geologic rates for some block bounding faults.

5.2. Fault Slip Rates

[26] Table 2 lists strike-slip and fault-normal rates for selected faults used to define the blocks shown in Figure 7 along with longer-term slip rates from geologic studies where available. In Figure 12 we plot the GPS estimate for fault slip rate from our preferred block model versus the average geologic slip rate reported in the literature. Uncertainties on the geologic rates reflect the range of slip estimates reported and their uncertainties. The GPS-derived slip rates are upper bounds since they do not account for

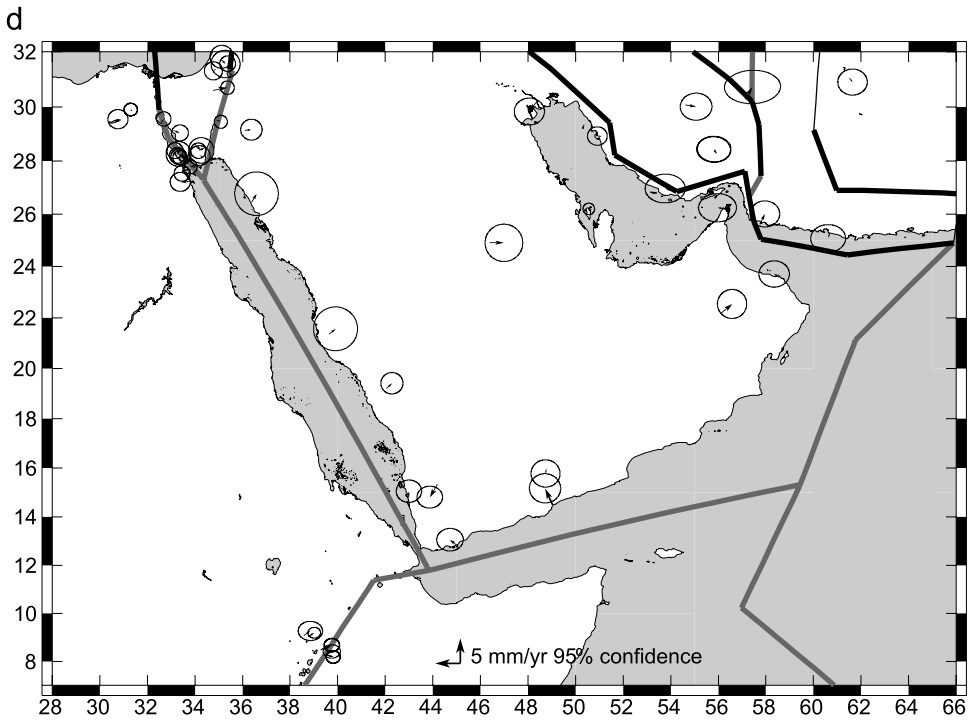

Figure 8. (continued)

possible permanent deformation of the blocks and all slip is assumed to occur on a single fault. In addition, because inversions of geodetic data for coseismic fault slip indicate that surface offsets are significantly less than offsets at seismogenic depths [e.g., *Feigl et al.*, 2002; *Delouis et al.*, 2002], geologic estimates provide a lower bound on fault slip rates.

[27] It is difficult to draw definitive conclusions about the relationship between present-day rates of faulting and longer-term geological rates because of the large uncertainties on most geologic estimates [e.g., *Allen et al.*, 2004] and the lack of detailed, near fault GPS coverage for many structures. The best determined geologic rates are for Red Sea and Gulf of Aden spreading since these are derived from mapped magnetic anomalies with well-determined ages [*Chu and Gordon*, 1998, 1999]. In these cases, there is close agreement between both the rates and directions of GPS and geologic estimates (Table 2) [see also *McClusky et al.*, 2003]. The North Anatolian, East Anatolian, Dead Sea, Gulf of Suez, Mosha, and Pembak-Sevan-Sunik faults all have geodetic and geologic slip rates that agree within 1σ uncertainties. Long-term slip rates for the NAF may be somewhat lower than present-day slip rates [e.g., *Şengör et al.*, 2004, Figure 23], although uncertainties on the timing of initiation of the fault and possible off-fault deformation [*Şengör et al.*, 2004; *Westaway*, 2004] complicate these comparisons.

[28] The Zagros Main Recent fault [*Vernant et al.*, 2004a] and the Gulf of Corinth show significant differences between geodetic and geologic slip rates. The geologic strike-slip rate (averaged over 3–5 Myr) for the Zagros Main Recent fault in particular is a factor of 3–5 greater than the geodetic rate [*Talebian and Jackson*, 2002; *Bachmanov et al.*, 2004]. Even with the absence of direct control on the age of the fault, this difference seems difficult to ascribe to uncertainties in the geologic rate. Similarly, fault-normal extension on the main fault along the southern side of the Gulf of Corinth determined from geologic observations [*Armijo et al.*, 1996] averaged over 350 kyr are significantly less than the geodetic rate. This difference is difficult to ascribe to uncertainties in the geologic estimates, and may reflect temporal variations in fault activity [*Jackson*, 1999]. However, definitive conclusions are difficult since the geodetic determination is not that well constrained and likely integrates deformation over a substantially wider area than the single geologic fault estimate.

[29] While uncertainties on fault slip rate estimates are generally too high to clearly define variations in slip rates with time, GPS slip rates are mostly comparable to geologic estimates (Figure 12), and geologically active faults account for present-day block motions and regional deformation. This agreement, the consistent geodetic and geologic Euler vectors for Arabia-Nubia, Arabia-Somalia, and Somalia-Nubia, and the agreement between geologic and geodetic estimates of Nubia-Eurasia and Arabia-Eurasia relative motions suggests to us that the GPS results reflect the same geologic processes operating in the region during the most recent geologic period (~3–5 Ma).

5.3. Accommodation of Arabia-Eurasia Continental Collision

[30] The collision of Arabia with Eurasia results in a reduction in the area of lithosphere within the deforming region caught in the collision zone. This reduction occurs via lateral transport of lithosphere out of the collision zone and by lithospheric shortening, presumably associated with thickening of the trapped lithosphere [e.g., *McKenzie*, 1972]. The block model allows quantitative estimation of

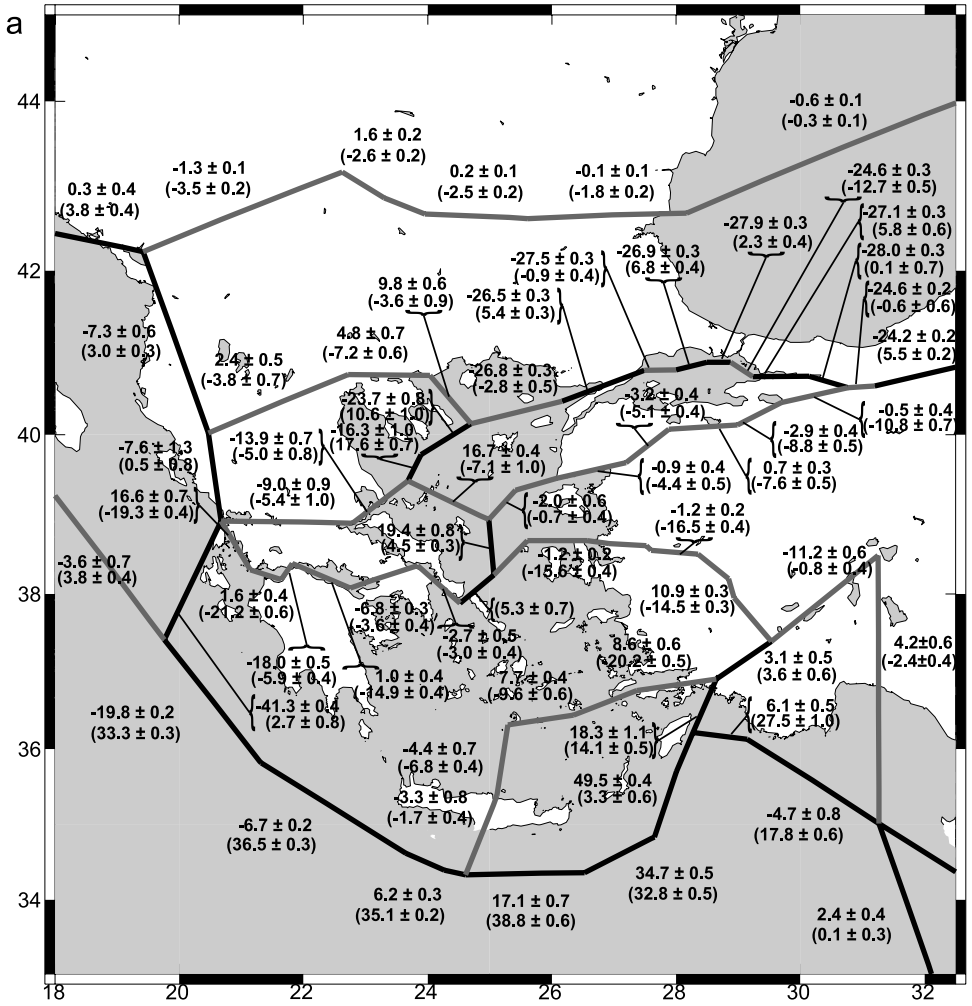

Figure 9. Maps showing fault slip rates (mm/yr) deduced from the block model shown in Figure 7. Top numbers (no parentheses) are strike-slip rates, positive being left-lateral. Numbers in parentheses are fault-normal slip rates, positive being closing. Slip rates are listed in Table S2.

the contribution of these processes. We use the absolute value of the rate of strike-slip faulting times fault length, and fault-normal motion rate times fault length (positive for convergence) summed over all block-bounding faults in the collision zone between the Dead Sea fault and the Caspian Sea (36°–50°E; 36°–43°N) as proxies for the contributions of lateral transport and lithospheric thickening/thinning, respectively. We find a rate of lateral transport of area within the collision zone of approximately 31 $\times$ 10^3 km^2/Myr. About 14 $\times$ 10^3 km^2/Myr corresponds to the rate of surface area consumed (i.e., by fault-normal convergence) of which about 5 $\times$ 10^3 km^2/Myr is consumed along the Main Caucasus Thrust, and 1 $\times$ 10^3 km^2/Myr along the northern Zagros Thrust. About 5 $\times$ 10^3 km^2/Myr of area is produced by extension in the collision zone. This leaves very little decrease in area within the Lesser Caucasus/eastern Turkey region due to fault-normal convergence ($\sim$3 $\times$ 10^3 km^2/Myr), indicating that only about 10% of the convergence of Arabia with Eurasia is accommodated by lithospheric shortening in the interior part of the collision zone. This analysis is born out by the remarkably uniform velocities along the 150 km long profile segment crossing the Lesser Caucasus (Figure 4e). Most of the decrease in surface area is being accommodated by shortening along the Caucasus and Zagros thrusts on the northern and eastern margins of the collision zone ($\sim$15%) and by lateral transport out of the collision zone ($\sim$70%). The predominance of lateral crustal transport and localized extension in the eastern Turkey region has also been suggested from space imagery and in-field fault analyses [*Chorowicz et al.*, 1999].

[31] The absence of significant shortening within eastern Turkey and the Lesser Caucasus is surprising in light of geologic evidence for crustal shortening [e.g., *Şengör and Yilmaz*, 1981; *Lyberis et al.*, 1992], the regional high topography (average >2 km), and dynamic extrusion models that presume high N-S compressional stresses associated with collision of the Arabian promontory with Eurasia [e.g., *Şengör et al.*, 1985; *Philip et al.*, 1989]. On the other hand, the eastern Turkey high plateau and the Lesser Caucasus have been subject to substantial volcanism that postdates the initiation of continental collision [*Pearce et al.*, 1990]. This volcanism is not easily reconciled with large compressional stress in the crust that would be required to cause significant

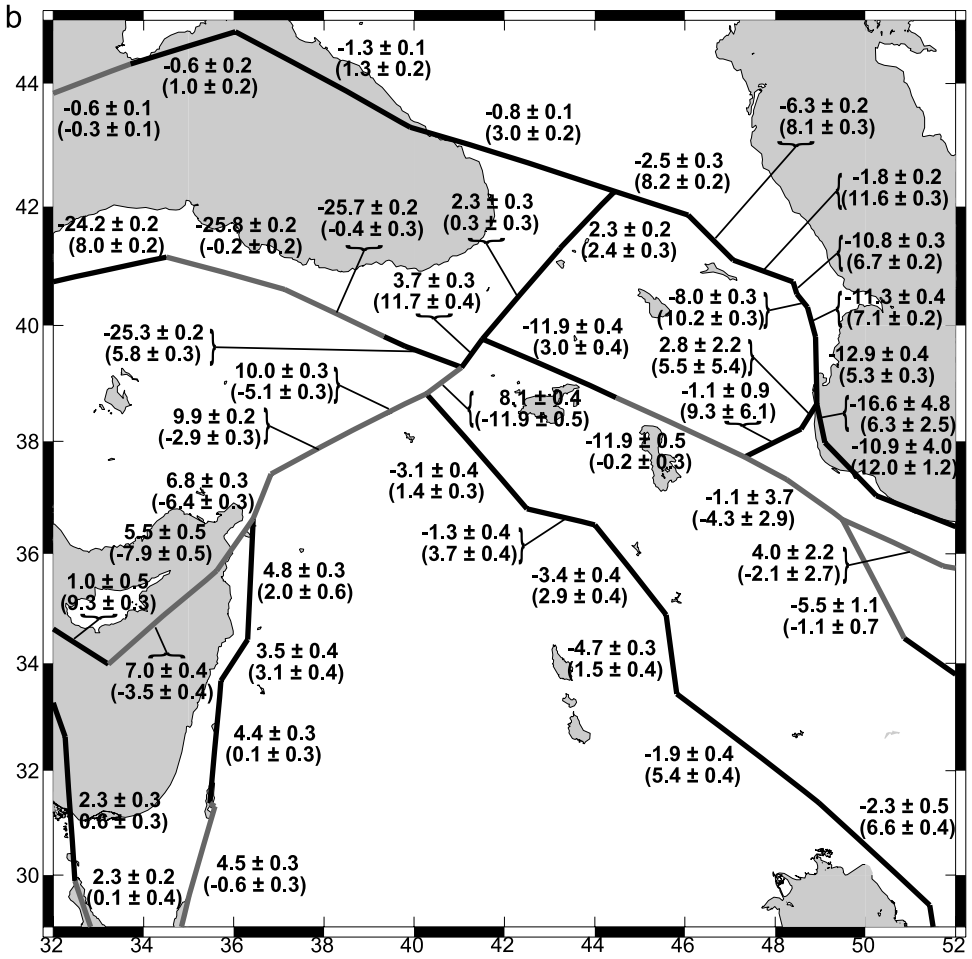

Figure 9. (continued)

crustal shortening [*Dhont et al.*, 1998]. In addition, recent seismic observations have been interpreted to indicate only slightly thickened crust in the collision zone [*Zor et al.*, 2003]. The slightly thickened crust, high topography, and results from seismic wave propagation studies have in turn been interpreted to indicate the absence of a high-density mantle lid and the presence of hot, low-density asthenosphere at the base of the crust [*Şengör et al.*, 2003]. These observations imply that the deformation zone along the southern edge of the Eurasian plate north of the Arabian promontory and south of the MCT has experienced only a small amount of shortening during the period of Arabian plate collision.

[32] The lack of substantial, present-day shortening within the Lesser Caucasus and apparent coherent motion of the Caucasus block indicated by the GPS results appear to contradict geologic evidence for distributed shortening [e.g., *Şengör and Yilmaz*, 1981; *Philip et al.*, 1989]. A similar "discrepancy" occurs in the Aegean where the GPS results indicate coherent motion with little internal deformation while there is substantial geologic evidence for widespread extension [e.g., *Armijo et al.*, 1996]. *McClusky et al.* [2000] suggest that the change from widespread extension to coherent plate translation in the Aegean might be related to propagation of the NAF across the North Aegean Trough during the last 3–5 Myr [see also *Flerit et al.*, 2004]. Prior to this time, the overriding Aegean region was part of Eurasia and trench rollback was accommodated by distributed extension in the back-arc region. Propagation of the NAF across the north Aegean decoupled the Aegean from Eurasia, concentrating deformation in the north Aegean and Gulf of Corinth and thereby allowing the central and southern Aegean and the Peloponnesus to move trenchward with little internal deformation. We suggest a similar scenario for the Lesser Caucasus–eastern Turkey region. Prior to the development of the NAF, Arabia–Eurasia convergence was accommodated primarily by lithospheric shortening and crustal thickening. With the development of the NAF and its eastward extension into the Lesser Caucasus and Iran, shortening south of the MCT ceased and was replaced by lateral escape of coherent lithospheric blocks with shortening being concentrated along the Main Caucasus and Zagros thrusts.

5.4. Some Implications for Plate Dynamics and Rheology

[33] Determining the contributions of the various forces to driving plate motions, and the rheology of the continental lithosphere (i.e., the response to these forces) are difficult problems involving trade-offs between forcing and rheology and a large number of poorly constrained parameters. However, the capability of GPS to map secular deformation

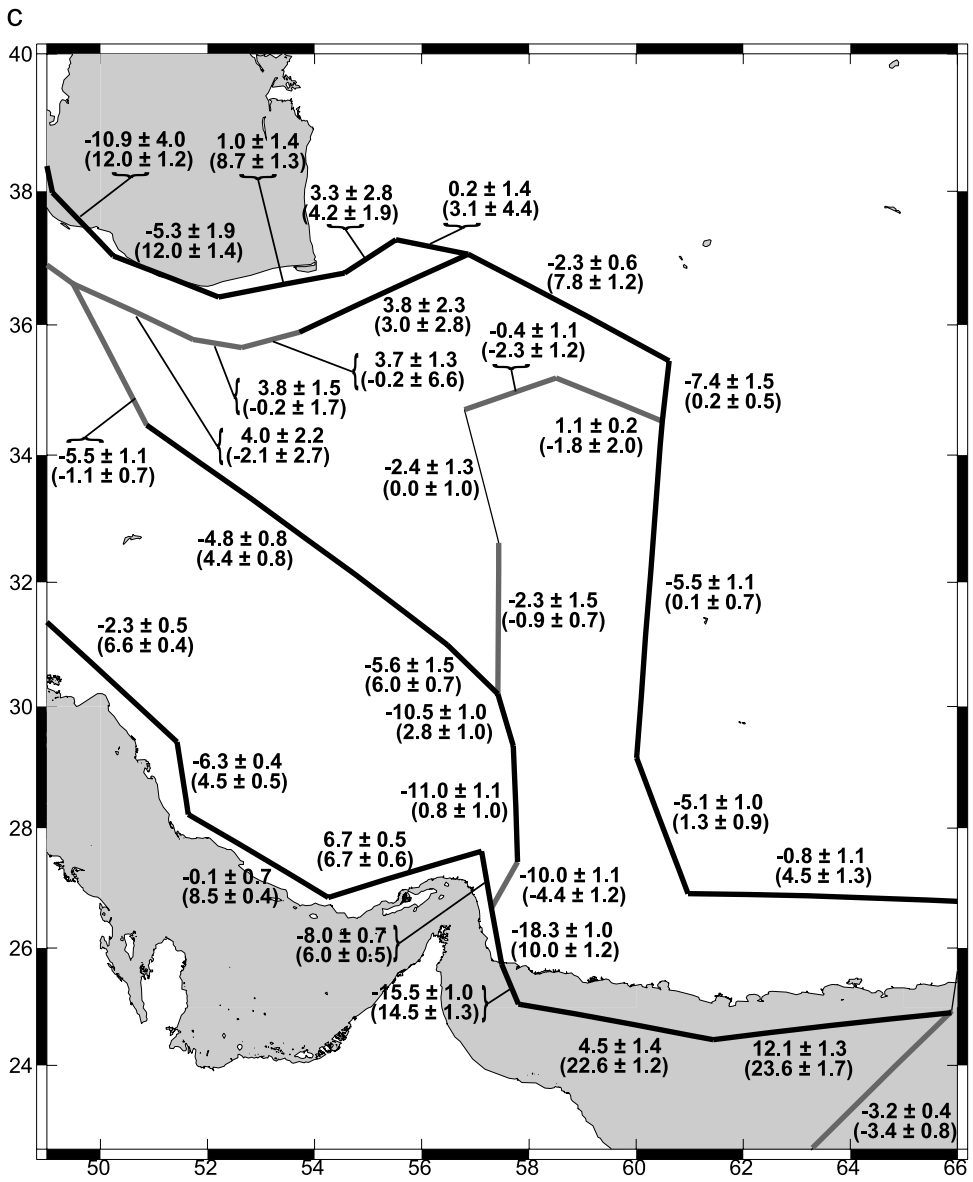

Figure 9. (continued)

to high precision (i.e., ≪ relative plate motions) at regional scales provides fundamentally new constraints that should limit the range of allowable dynamic and rheologic models. Furthermore, in the greater east Mediterranean we have captured the entire region of plate interaction in a single, internally consistent velocity field allowing us to compare deformation associated with the major tectonic features in the zone of plate interaction, comparisons that may lead to a better understanding of the relative importance of various tectonic processes in driving plate motions.

[34] The continuous increase in GPS velocities from northern most Arabia across Anatolia toward the Hellenic trench requires that any "pushing" of Anatolia by Arabia, as is implicit in the extrusion model [*Şengör et al.*, 1985] must be small or nonexistent to occur without any evidence of fault-normal shortening along the EAF or within the Anatolian plate. This observation alone is strong evidence against extrusion as a significant dynamic mechanism responsible for present-day Anatolia motion.

[35] Because the character of interaction between the Arabian and Anatolian plates in SE Anatolia is of critical importance for dynamic models of Anatolia motion, we investigate this further with a model that includes a separate eastern Turkey block (Figure 13). Our concern is that westward directed motions in western Turkey may bias the overall motion of Anatolia. The eastern Turkey block in the new model has a western boundary that follows the break in topography between the eastern Turkey high plateau and central Anatolia (compare Figures 1 and 13). *Kocyigit and Beyhan* [1998] proposed the existence of an active fault (Central Anatolia Fault Zone; CAFZ) in this approximate location with a left-lateral slip rate of 2–3 mm/yr. In contrast, *Westaway* [1999] suggested that this fault was currently inactive. Distinguishing between 0 and 2 mm/yr slip rates is difficult with the current data. Figure 13, however, indicates that slip on the NE-SW branch of the CAFZ is insignificant (0 ± 0.5 mm/yr) and adding this fault to the model does not significantly improve the fit to the

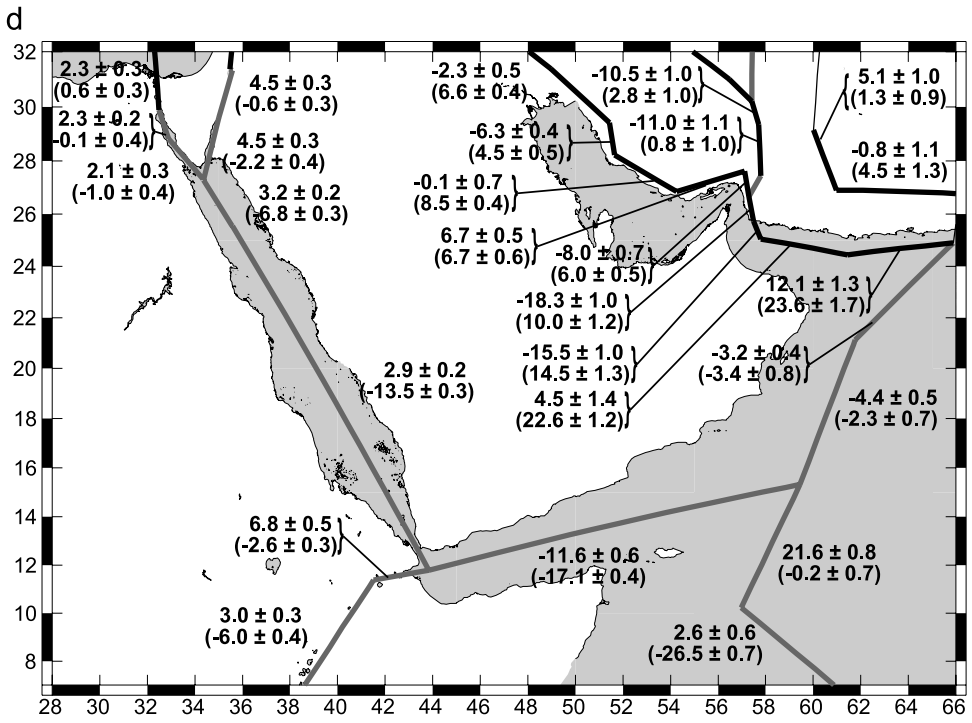

Figure 9. (continued)

observations. More important for our discussion of plate dynamics, the inclusion of an eastern Turkey block does not change our conclusion that the Arabia-Anatolia plate boundary is characterized by pure strike slip with no fault-normal compression and possibly small extension.

[36] The rapid trenchward motions along the Hellenic arc, in themselves, seem to require that subduction is fundamentally responsible for driving plate motions within the plate collision zone. Since the African plate is being subducted beneath the Aegean, these forces presumably arise from trench suction [*Conrad and Lithgow-Bertelloni*, 2004]. As the African lithosphere sinks beneath the Hellenic trench due to its negative buoyancy (trench roll-back [e.g., *Royden*, 1993]), the Aegean and Anatolian plates, and presumably the underlying mantle, are drawn into the volume of low pressure caused by the retreating slab. This "pulling" by the retreating slab induces motions with increasing rates toward the trench, as observed. This process apparently continues east along the western Cyprus trench where geologically recent extension of the overriding plate has been documented from a suite of marine geophysical data [*ten Veen et al.*, 2004].

[37] Rotation of the Arabian plate relative to Eurasia about a pole located near that for Anatolia (i.e., where the African plate is subducting in the Mediterranean; Table 1) raises the possibility that Arabian and Anatolian plate motions result from the same dynamic process, namely forces directly associated with the downgoing African lithosphere. Rotation of the Arabian plate may be aided by active subduction at the Makran trench and possibly beneath the south Zagros fold and thrust belt [*Bellahsen et al.*, 2003]. The dominance of fault-normal shortening along, and inboard of the Makran and south Zagros (Figure 9c) [*Vernant et al.*, 2004a] and the occurrence of extension

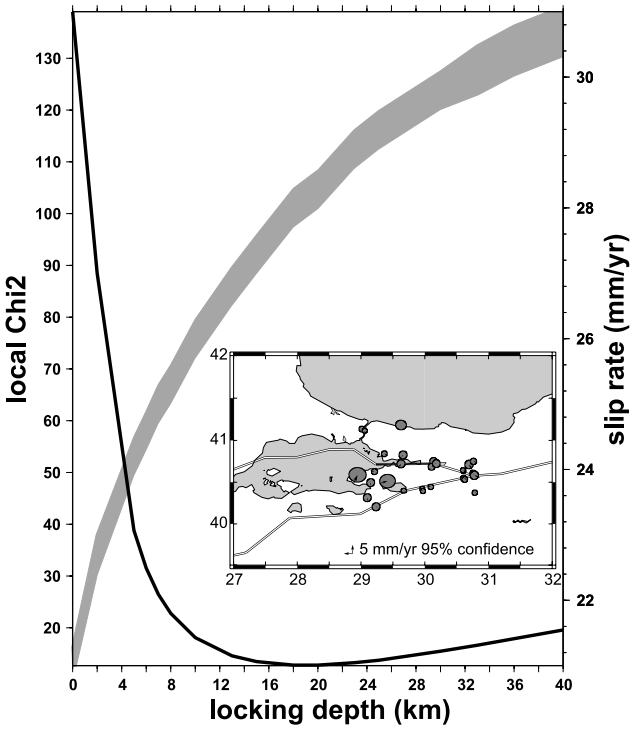

Figure 10. Local χ^2 (measure of how well the model fits the observations) and slip rate, plotted versus locking depth for the North Anatolian fault. Velocity residuals for GPS sites used to determine the local χ^2 are shown in the inset map. The best fit is for locking depths in the range 15–25 km, with slip rates varying from 27 to 29.2 mm/yr.

Table 2. GPS-Derived Fault Slip Rates Deduced From the Block Model Shown in Figure 7 for Selected Block-Bounding Faults and Geologic Slip Rates Where Available[a]

Fault[b]	GPS SS	GPS DS	GEO SS	GEO DS	REF[c]
NAF	−24 ± 1	−1/+7 ± 1	−16/−24 ± 5		h−f, w, arm, kz
EAF	10 ± 1	−3/−5 ± 1	−11 ± 2		w
DSF	4.5/4.8 ± 1[d]	−2/+2 ± 1[d]	4/7 ± 2		m, g, k, n, d, jg
Gulf of Suez	2 ± 1	0/−1 ± 1		−1	st, jg
Red Sea	3 ± 1	−7/−17 ± 1[e]	3 ± 2	−8/−18 ± 2	chu, jg
Gulf of Aden	−10/−13 ± 1	−12/−22 ± 1[f]		−16/−24 ± 5[f]	je, nu, gd, jg
Gulf of Corinth	2/−7 ± 1	−15/−21 ± 1		−11 ± 3	a96
Zagros FT	−2/3 ± 1	0/8 ± 1[e]	−10/17	10	t+j, b, ba
Hellenic (W)	−20/+6 ± 1[g]	38/44 ± 1[g]			
Hellenic (E)	17/50 ± 1[f]	3/39 ± 1[e]			
Cyprus (W)	−5/+1 ± 1	9/18 ± 1			
Cyprus (E)	7 ± 1	−4/−8 ± 2[f]			
Tabriz	−11 ± 1.5	−1.5			
Chalderan	−12 ± 1	0 ± 1			
Mosha	4 ± 1	0 ± 1	2.7 ± 0.5		r
PSSF[h]	−3.4 ± 1	0/−1.5 ± 1	−3/−4		tr, ph

[a]GPS SS, GPS strike-slip rate (left-lateral plus); GPS DS, GPS fault-normal rate (convergence plus); GEO SS, geological strike-slip rate; GEO DS, geological fault-normal rate; REF, geological reference. See Figures 9a–9d and Table S2 for more complete compilations. GPS slip rate uncertainties are formal, 1σ uncertainties from our block model rounded up to the nearest mm/yr.

[b]NAF, North Anatolian fault; EAF, East Anatolian fault; DSF, Dead Sea fault; PSSF, Pambak-Sevan-Sunik fault.

[c]References are a96, *Armijo et al.* [1996]; arm, *Armijo et al.* [1999]; ba, *Bachmanov et al.* [2004]; b, *Blanc et al.* [2003]; chu, *Chu and Gordon* [1998]; d, *Daeron et al.* [2004]; g, *Gomez et al.* [2003]; h–f, *Hubert-Ferrari et al.* [2002]; je, *Jestin et al.* [1994]; jg, *Joffe and Garfunkel* [1987]; k, *Klinger et al.* [2000]; kz, *Kozaci et al.* [2005]; m, *Meghraoui et al.* [2003]; n, *Niemi et al.* [2001]; nu, *DeMets et al.* [1990, 1994]; ph, *Philip et al.* [2001]; r, *Ritz et al.* [2006]; st, *Steckler et al.* [1998]; t+j, *Talebian and Jackson* [2002]; tr, *Trifonov et al.* [1994]; w, *Westaway* [1994].

[d]Increasing from south to north.

[e]Increasing from north to south.

[f]Increasing from SW to NE.

[g]Strike-slip increasing from SE to NW and fault-normal increasing from NW to SE.

[h]See Figure 11 for fault geometry.

along the northern Owens Fracture Zone (Arabia-India plate boundary, Figures 1b and 9d) are at least consistent with the subducting slab "pulling" the Arabian plate toward the NE. According to this conceptual model, the retreating slab in the eastern Mediterranean (Hellenic/Cyprus trenches) induces the overriding Aegean and Anatolian plates to move toward the trench while the subducting slab beneath the Makran and south Zagros imparts a pull to the Arabian plate

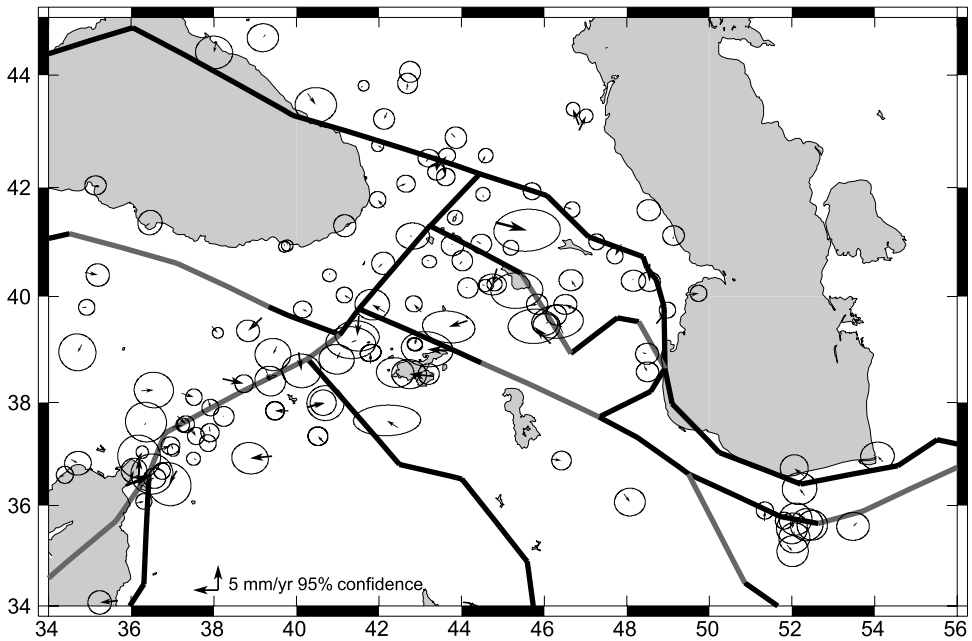

Figure 11a. Residual GPS velocities and 95% confidence ellipses for a block model including two blocks for the eastern Turkey Plateau–Lesser Caucasus. Model fault parameters are given in Table S2. Format is as in Figure 8.

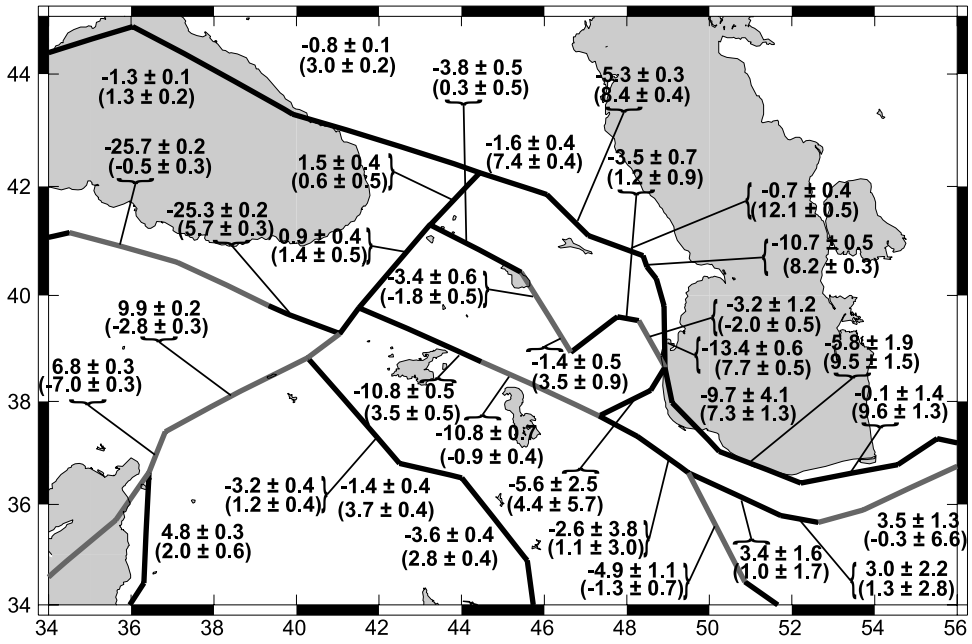

Figure 11b. Fault slip rates resulting from the block model shown in Figure 11a. Model slip rates are given in Table S2. Format is as in Figure 9.

toward the NNE. This combination of forces produces the observed counterclockwise rotations of Anatolia and Arabia and the rapid trenchward motion of the Aegean. "Ridge push" along the Red Sea and/or Gulf of Aden rifts is unlikely to play a significant role in driving motion of the Arabian plate given the narrow width of new ocean lithosphere, although forcing associated with the Afar plume interacting with the continental lithosphere may play some role. While we see no evidence of NE oriented compression within the Arabian plate, as would be expected if the Arabian plate is being "driven" by ridge push or by the Afar plume into Eurasia along the Makran and south Zagros (versus being pulled by the subducting slab), GPS velocity uncertainties are presently too large to rule this out.

[38] If our association of block motions with subduction is generally applicable to the entire zone of plate interaction, the relatively rapid NNE motions in the eastern Caucasus (Figure 3) suggest the presence of subduction beneath the Caucasus and perhaps the central Caspian Sea [*Jackson et al.*, 2002; *Vernant and Chery*, 2006]. While significant fault-normal shortening occurs along both the north Zagros and MCT, our block models indicate very little shortening and perhaps small fault-normal extension within the Lesser Caucasus and south of the Caspian Sea (Figures 9b, 9c, and 11), somewhat analogous to extension in western Anatolia juxtaposed with compression along the Hellenic and Cyprus trenches.

[39] While the kinematics appear to implicate processes associated with subduction as the principal source of surface deformation, how slab retreat and slab pull are imparted to the lithosphere remains uncertain. Are tensional forces transmitted through the plates or does subduction induce flow in the mantle that is imparted to the plates through shear tractions on the asthenosphere-lithosphere interface (or some combination of these processes)? The spatial scale of the observed, circulatory pattern of surface deformation (~3000 km) may favor a deep source, although the scale of deformation could be due to the dimensions of the Anatolian and Arabian plates. However, this leaves open the question of why the lithosphere responds to the dynamic processes by forming plates of this scale (lithospheric

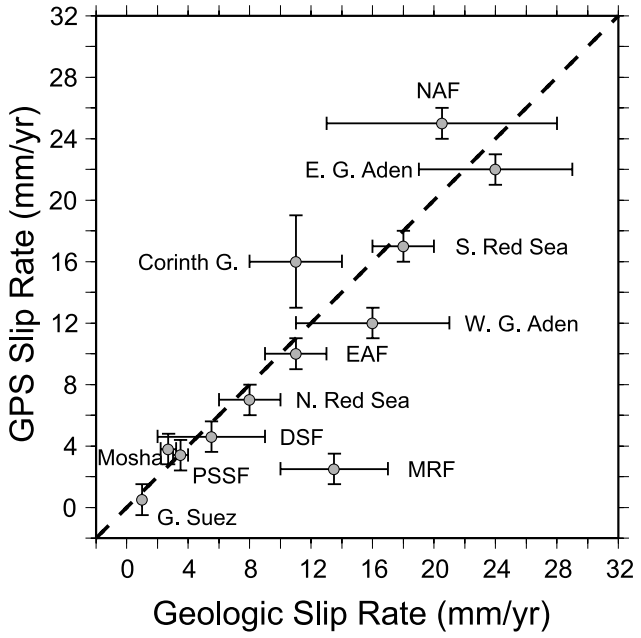

Figure 12. Plot of fault slip rates deduced from our preferred GPS-constrained block model (Figures 7 and 9 and Table S2) versus geologic slip rates reported in the literature (fault abbreviations and references are given in Table 2; we compare the GPS strike-slip rate for the Zagros FT with geologic strike-slip rates reported for the Main Recent fault (MRF)). We plot average of the more recent geologic rates with the uncertainty reflecting the range of rates reported.

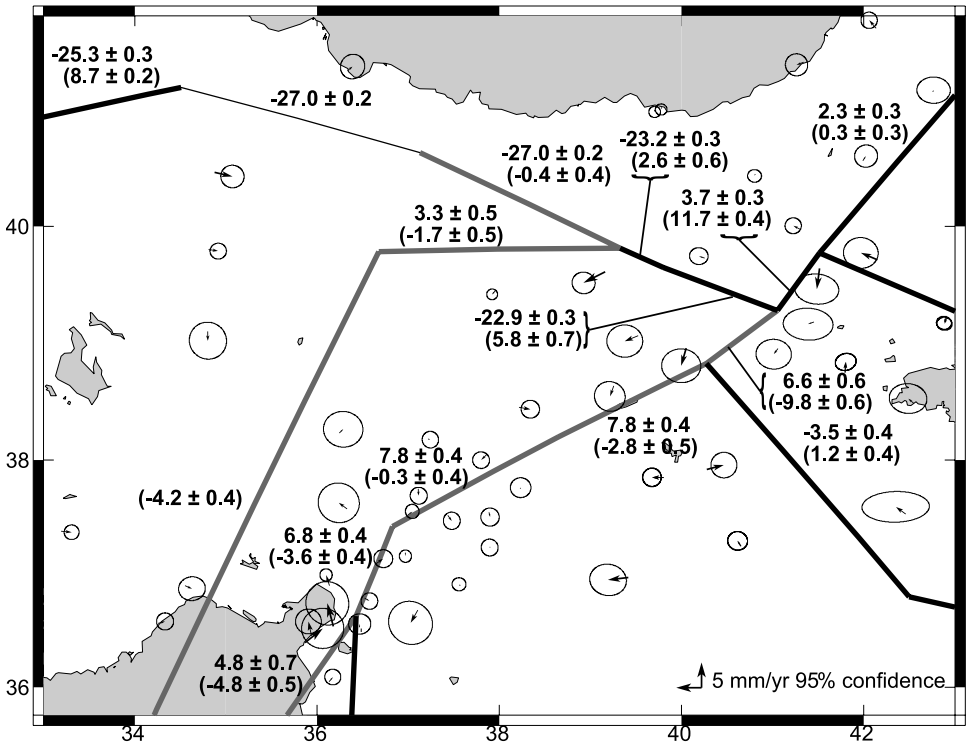

Figure 13. Map showing revised block model including an eastern Turkey block, residual velocities from this model, and deduced fault slip rates (same format as Figures 8 and 9). Model fault parameters are given in Table S2.

weakening associated with the interaction of the Afar plume with Africa/Arabia plate [e.g., *Bellahsen et al.*, 2003]?). Perhaps relevant to this discussion is the apparent balance between surface area consumed at trenches and along thrust faults ($\sim 112 \times 10^3$ km^2/Myr) and that created at ridges and at normal faults ($\sim 105 \times 10^3$ km^2/Myr) for the entire area of plate interaction (19–66°E; 12–46°N). This balance indicates that deformation in the Nubia-Somalia-Eurasia interplate region forms a roughly closed system. This is at least consistent with a dynamic "connection" between downwelling at trenches and upwelling at ridges. Whether this connection is via subduction pulling open the Red Sea and Gulf of Aden rifts (i.e., stresses transmitted through the lithosphere), or flow in the mantle from subduction zones toward ridges remains unresolved.

[40] While dynamic models that involve trench suction, slab pull, and/or sublithospheric mantle flow may require less strength in the lithosphere than extrusion models, coherent block and plate motions would appear to require a relatively strong continental lithosphere. The observation that the elastic block model provides a good fit to the GPS results and that the deduced GPS fault slip rates are comparable to geologic rates supports the notion that the crust has sufficient strength to behave elastically over geologic timescales (i.e., relative block motions are primarily accommodated by repeated cycles of elastic strain accumulation and release on block-bounding faults). In addition, the lack of continuing postseismic deformation from the sequence of $M > 7.5$ earthquakes along the NAF system during the last century supports models with high mantle viscosities (>5×10^{20} Pa s [*Hearn et al.*, 2002a]). Further support for a relatively strong lithosphere comes from the pattern of elastic strain accumulation along the NAF segment that broke in the M7.4, 1999 Izmit earthquake (Figure 5). Lithospheric models that include an elastic layer over a sufficiently low viscosity (i.e., weak) Maxwell viscoelastic layer predict a broadening of the strain field adjacent to strike-slip faults late in the earthquake cycle [*Savage and Prescott*, 1978; *Meade and Hager*, 2005]. The profile across the NAF shown in Figure 5 is based on GPS observations during a 10-year period immediately before the Izmit event, very late in the earthquake cycle. The excellent fit for an elastic half-space model with an ~20 km locking depth implies a relatively high viscosity ($\sim 10^{20}$ Pa s) for the lower crust/upper mantle in NW Turkey (see *Meade and Hager* [2005] for quantitative discussion). The notion that blocks in the collision zone have significant strength is further supported by the absence of a correlation between topographic relief in eastern and central Turkey and surface deformation (i.e., no significant deformation across the step in topography between eastern and central Anatolia; compare Figures 1 and 13). This argues against internal, gravitationally driven body forces contributing significantly to the dynamics of Anatolia plate motion [see also *Provost et al.*, 2003] and for a sufficiently strong crust capable of maintaining stresses associated with large gravitational potential energy differences.

6. Conclusions

[41] The principal result of this study is the GPS-derived, secular velocity field for the period 1988–2005 in the zone of interaction of the Nubian, Somalian, Arabian, and Eurasian plates (Figures 2 and 3 and Table S1). Our main

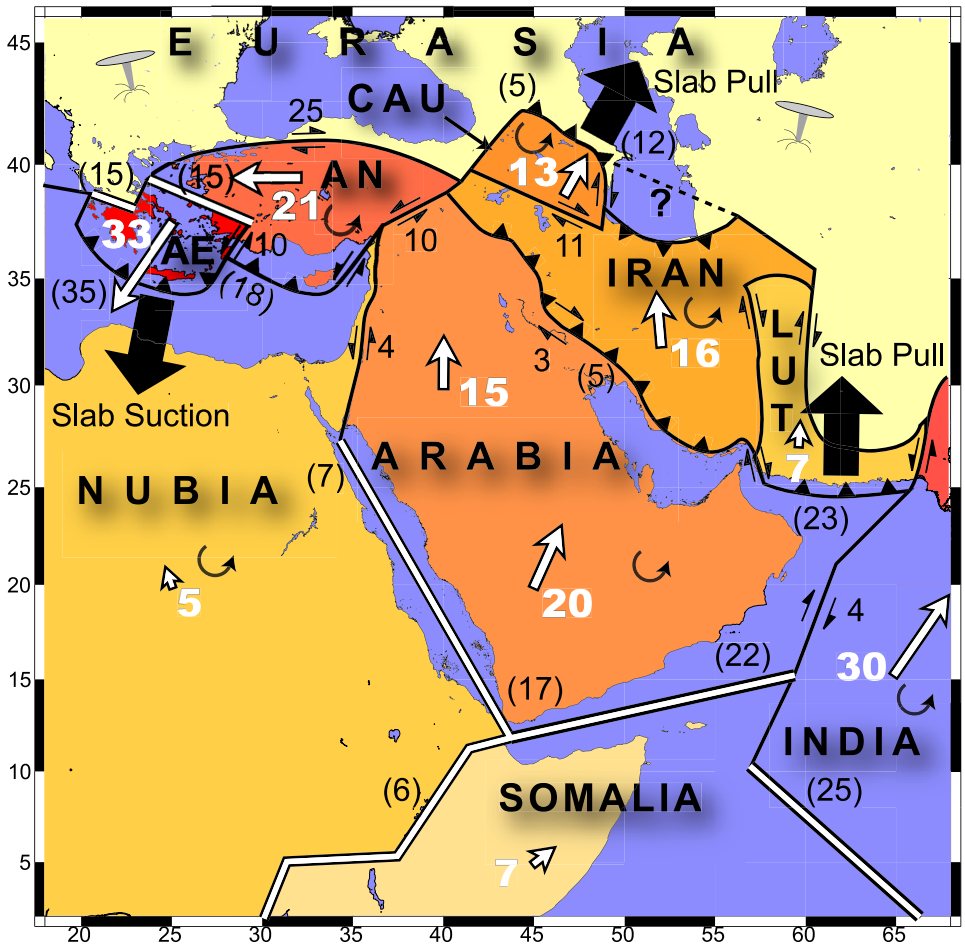

Figure 14. Schematic map of the Arabia-Africa-Eurasia zone of plate interaction illustrating the principal results of this study. Names refer to plates and blocks (CAUC, Caucasus block; AN, Anatolia plate; AE, Aegean plate). Double lines are extensional plate boundaries, plain lines are strike-slip boundaries (paired arrows show direction of strike-slip motion), and lines with triangles are thrust faults. Dark numbers are GPS-derived slip rates (mm/yr) on block-bounding faults (numbers in parentheses are dip slip and those without are strike slip). White arrows and corresponding numbers show GPS-derived plate velocities (mm/yr) relative to Eurasia. Curved arrows show sense of block rotation relative to Eurasia. Dark, heavy arrows show hypothesized forces associated with active subduction acting on the plate/block system and causing counterclockwise rotation of Arabia-central Iran-Anatolia-Aegean relative to Eurasia.

conclusions based on these new results are illustrated schematically in Figure 14. The velocity field indicates counterclockwise rotation of a broad area including the Arabian, Anatolian, and Aegean regions and adjacent parts of the Zagros and central Iran. Rates of motion associated with this rotation increase toward the Hellenic-Cyprus trench system. The velocity field is characterized well by a system of undeforming regions separated by concentrated zones of deformation (widths $\ll$100 km). Deformation zones correlate closely with mapped, active faults and historic seismicity, and coherent regions with seismically quiet zones, qualitatively consistent with the original plate tectonic, kinematic models for this region [*McKenzie*, 1970; *McKenzie et al.*, 1970]. We use a simple, kinematic block model, including elastic strain accumulation on block-bounding faults, to quantify relative block motions (Table 1) and to determine present-day rates of strain accumulation on block-bounding faults (modeled as deep fault slip). The GPS-derived Euler vectors for Arabia-Nubia, Somalia-Nubia, and Arabia-Somalia are in good agreement with the most recent geologic Euler vectors derived from plate reconstructions. In addition, the GPS-derived relative motions between Nubia and Eurasia, and Arabia and Eurasia are consistent with the most recent geologic estimates. We also find that, with some exceptions, the estimated GPS slip rates for major block-bounding faults are comparable to geologic rates estimated for the past few million years (Table 2 and Figure 12), most often differing by less than 1σ uncertainties. These comparisons indicate that the GPS velocity field characterizes accurately deformation in the zone of plate interaction during the late Pliocene ($\sim$3–5 Ma).

[42] Within the zone of active continental collision in eastern Turkey and the Lesser Caucasus, we find that lateral

transport of lithosphere out of the zone of plate convergence and shortening along the Main Caucasus Thrust are the predominant processes accommodating Arabia-Eurasia convergence. Furthermore, the boundary between the Arabian plate and the Anatolian plate is characterized by predominantly left-lateral strike-slip motion with no fault-normal convergence and possibly a small amount of extension. These kinematic results rule out "extrusion" as a dynamic mechanism for present-day westward motion and counterclockwise rotation of the Anatolian plate. The increasing rate of motion toward the Hellenic and Cyprus trenches suggests to us that the primary forces responsible for westward motion of Anatolia, and perhaps counterclockwise rotation of Arabia, are associated with slab rollback along the Hellenic and Cyprus trenches. Counterclockwise rotation of the Arabian plate may be enhanced by slab pull from NE-directed subduction beneath the Makran and possibly the south Zagros. A direct corollary of this proposed dynamic hypothesis is that rifting in the Red Sea and Gulf of Aden is a response to plate motions induced by active subduction. This interpretation implies that continuing subduction of the African and Arabian oceanic lithosphere (i.e., Neotethys) is driving plate motions and interplate deformation throughout the zone of interaction of the African, Arabian, and Eurasian plates.

[43] **Acknowledgments.** We are grateful to the many individuals who participated in GPS surveys over the past 15 years, to those individuals and institutions that support the global IGS network, and to UNAVCO and the Turkish General Command of Mapping for technical support for GPS surveys and continuous GPS station installation and maintenance. Becky Bendick and Pierre Briolle provided published GPS data around the East African rift and Gulf of Corinth, respectively. We benefited from discussions with Mark Allen, Muawia Barazangi, Michael Bevis, Jean Chery, Bradford Hager, Laurent Husson, James Jackson, Sadi Kuleli, Brendon Meade, and Nafi Toksoz on regional geodynamics and with Thomas Herring and Robert King on GPS data analysis. We obtained both IGS tracking data and global analyses (solution files) from the Scripps Orbit and Permanent Array Center. The maps in this paper were generated using the public domain Generic Mapping Tools (GMT) software [*Wessel and Smith*, 1995]. We are grateful for formal reviews that improved the manuscript by Charles DeMets, Timothy Dixon, and Shimon Wdowinski. We especially acknowledge the pioneering work on this project by the late Aykut Barka in Turkey and the late Serguei Balassanian in Armenia. This research was supported in part by NSF grants EAR-0337497, EAR-0305480, and INT-0001583 and NASA grant NNG04GA15G.

References

Allen, M., J. Jackson, and R. Walker (2004), Late Cenozoic reorganization of the Arabia-Eurasia collision and the comparison of short-term and long-term deformation rates, *Tectonics*, *23*, TC2008, doi:10.1029/2003TC001530.

Armijo, R., H. Lyon-Caen, and D. Papanastassiou (1992), East-west extension and Holocene normal fault scarps in the Hellenic arc, *Geology*, *20*, 492–494.

Armijo, R., B. Meyer, G. C. P. King, A. Rigo, and D. Papanastassiou (1996), Quaternary evolution of the Gulf of Corinth rift and its implications for the Late Cenozoic evolution of the Aegean, *Geophys. J. R. Astron. Soc.*, *126*, 11–53.

Armijo, R., B. Meyer, A. Hubert, and A. Barka (1999), Propagation of the North Anatolian fault into the north Aegean: Timing and kinematics, *Geology*, *27*, 267–270.

Bachmanov, D. M., et al. (2004), Active faults in the Zagros and central Iran, *Tectonophysics*, *380*, 221–241.

Bellahsen, N., C. Faccenna, F. Funiciello, J. M. Daniel, and L. Jolivet (2003), Why did Arabia separate from Africa? Insights from 3-D laboratory experiments, *Earth and Plan Sci. Lett.*, *216*, 365–381, doi:10.1016/S0012-821X(03)00516-8.

Bendick, R., S. McClusky, R. Bilham, L. Asfaw, and S. Klemper (2005), Distributed Nubia-Somalia relative motion and dike intrusion in the Main Ethiopia Rift, *Geophys. J. Int.*, *165*, 303–310.

Blanc, E. J.-P., M. B. Allen, S. Inger, and H. Hassani (2003), Structural styles in the Zagros Simple Folded Zone, Iran, *J. Geol. Soc. London*, *160*, 401–412.

Bock, Y., J. Behr, P. Fang, J. Dean, and R. Leigh (1997), Scripps Orbit and Permanent Array Center (SOPAC) and Southern California Permanent GPS Array (PGGA), in *The Global Positioning System for the Geosciences*, pp. 55–61, Natl. Acad. Press, Washington, D. C.

Bozkurt, E. (2003), Origin of NE-trending basins in western Turkey, *Geodin. Acta*, *16*, 61–81.

Calais, E., C. De Mets, and J. M. Nocquet (2003), Evidence of a post-3.16 Ma change in Nubia-Eurasia plate motion, *Earth Planet. Sci. Lett.*, *216*, 81–92.

Chorowicz, J., D. Dhont, and N. Gundogdu (1999), Neotectonics in the eastern North Anatolian fault region (Turkey) advocates crustal extension: Mapping from SAR ERS imagery and Digital Elevation Model, *J. Struct. Geol.*, *21*, 511–532.

Chu, D., and G. Gordon (1998), Current plate motions across the Red Sea, *Geophys. J. Int.*, *135*, 313–328.

Chu, D., and G. Gordon (1999), Evidence for motion between Nubia and Somalia along the Southwest Indian ridge, *Nature*, *398*, 64–66.

Clarke, P. J., et al. (1998), Crustal strain in central Greece from repeated GPS measurements in the interval 1989–1997, *Geophys. J. Int.*, *135*, 195–214.

Conrad, C. P., and C. Lithgow-Bertelloni (2004), The temporal evolution of plate driving forces: Importance of "slab suction" versus "slab pull" during the Cenozoic, *J. Geophys. Res.*, *109*, B10407, doi:10.1029/2004JB002991.

Daeron, M., L. Benedetti, P. Tapponier, A. Sursock, and R. C. Finkel (2004), Constraints on the post ~25-ka slip rate of the Yammouneh fault (Lebanon) using in situ cosmogenic ^{36}CL dating of offset limestone-clast fans, *Earth Planet. Sci. Lett.*, *227*, 105–119.

Davies, R., P. England, B. Parsons, H. Billiris, D. Paradissis, and G. Veis (1997), Geodetic strain in Greece in the interval 1892–1992, *J. Geophys. Res.*, *102*, 24,571–24,588.

Delouis, B., D. Giardini, P. Lundgren, and J. Salichon (2002), Joint inversion of InSAR, GPS, teleseismic, and strong-motion data for the spatial and temporal distribution of earthquake slip: Application to the 1999 Izmit mainshock, *Bull. Seismol. Soc. Am.*, *92*, 278–299.

DeMets, C., R. G. Gordon, D. F. Argus, and S. Stein (1990), Current plate motions, *Geophys. J. Int.*, *101*, 425–478.

DeMets, C., R. G. Gordon, D. F. Argus, and S. Stein (1994), Effects of recent revisions to the geomagnetic reversal time scale on estimates of current plate motions, *Geophys. Res. Lett.*, *21*, 2191–2194.

Dhont, D., J. Chorowicz, T. Yurur, and O. Kose (1998), Polyphased block tectonics along the North Anatolian Fault in the Tosya basin area (Turkey), *Tectonophysics*, *299*, 213–227.

Dong, D., T. A. Herring, and R. W. King (1998), Estimating regional deformation from a combination of space and terrestrial geodetic data, *J. Geod.*, *72*, 200–211.

Dorbath, L., and A. Cisternas (1997), Recent great earthquakes in the Caucasus region, in *Historical and Prehistorical Earthquakes in the Caucasus*, edited by D. Giardini and S. Balassanian, pp. 401–441, Springer, New York.

Elsasser, W. M. (1971), Sea-floor spreading as thermal convection, *J. Geophys. Res.*, *76*, 1101–1112.

England, P. C., and D. P. McKenzie (1983), A thin viscous sheet model for continental deformation, *Geophys. J. R. Astron. Soc.*, *73*, 523–532.

Ergintav, S., et al. (2002), Postseismic deformation near the Izmit earthquake (08/17/99, M = 7.5) rupture zone, *Bull. Seismol. Soc. Am.*, *92*, 194–207.

Feigl, K., et al. (2002), Estimating slip distribution for the Izmit main shock from coseismic GPS, SPOT, and ERS-1 measurements, *Bull. Seismol. Soc. Am.*, *92*, 161–171.

Fernandez, R. M. S., B. A. C. Ambrosius, R. Noomen, L. Bastos, M. J. R. Wortel, W. Spakman, and R. Govers (2003), The relative motion between Africa and Eurasia as derived from ITRF2000 and GPS data, *Geophys. Res. Lett.*, *30*(16), 1828, doi:10.1029/2003GL017089.

Fernandez, R. M. S., B. A. C. Ambrosius, R. Noomen, L. Bastos, L. Combrinck, J. M. Miranda, and W. Spakman (2004), Angular velocities of Nubia and Somalia from continuous GPS data: Implications on present-day relative kinematics, *Earth Planet. Sci. Lett.*, *222*, 197–208, doi:10.1016/j.epsl.2004.02.008.

Flerit, F., R. Armijo, G. King, and B. Meyer (2004), The mechanical interaction between the propogating North Anatolian fault and the back-arc extension in the Aegean, *Earth Planet. Sci. Lett.*, *224*, 347–362.

Gelb, A (1974), *Applied Optimal Estimation*, MIT Press, Cambridge, Mass.

Goldsworthy, M., J. Jackson, and J. Haines (2002), The continuity of active fault systems in Greece, *Geophys. J. Int.*, *148*, 596–618.

Gomez, F., et al. (2003), Holocene faulting and earthquake recurrence along the Serghaya branch of the Dead Sea fault system in Syria and Lebanon, *Geophys. J. Int.*, *153*, 658–674.

Gordon, R. G., and C. DeMets (1989), Present-day motion along the Owen Fracture Zone and Dalrymple Trough in the Arabian Sea, *J. Geophys. Res.*, *94*, 5560–5570.

Hager, B. H., R. W. King, and M. H. Murray (1991), Measurements of crustal deformation using the Global Positioning System, *Annu. Rev. Earth Planet Sci.*, *19*, 351–382.

Hearn, E. H., B. H. Hager, and R. E. Reilinger (2002a), Viscoelastic deformation from North Anatolian Fault Zone earthquakes and the eastern Mediterranean GPS velocity field, *Geophys. Res. Lett.*, *29*(11), 1549, doi:10.1029/2002GL014889.

Hearn, E. H., R. Burgmann, and R. E. Reilinger (2002b), Dynamics of Izmit earthquake postseismic deformation and loading of the Düzce earthquake hypocenter, *Bull. Seismol. Soc. Am.*, *92*, 172–193.

Herring, T. A. (2004), GLOBK: Global Kalman filter VLBI and GPS analysis program version 4.1, Mass. Inst. of Technol., Cambridge.

Hubert-Ferrari, A., A. Barka, E. Jacques, S. Nalbant, B. Meyer, R. Armijo, P. Tapponier, and G. C. P. King (2000), Seismic hazard in the Marmara Sea region following the 17 August 1999 Izmit earthquake, *Nature*, *404*, 269–271.

Hubert-Ferrari, A., R. Armijo, G. King, B. Meyer, and A. Barka (2002), Morphology, displacement, and slip rates along the North Anatolian fault, Turkey, *J. Geophys. Res.*, *107*(B10), 2235, doi:10.1029/2001JB000393.

Isacks, B., J. Oliver, and L. R. Sykes (1968), Seismology and the new global tectonics, *J. Geophys. Res.*, *73*, 5855–5899.

Jackson, J. (1992), Partitioning of strike-slip and convergent motion between Eurasia and Arabia in eastern Turkey, *J. Geophys. Res.*, *97*, 12,471–12,479.

Jackson, J. (1999), Fault death: A perspective from actively deforming regions, *J. Struct. Geol.*, *21*, 1003–1010.

Jackson, J., and D. McKenzie (1984), Active tectonics of the Alpine-Himalayan belt between western Turkey and Pakistan, *Geophys. J. R. Astron. Soc.*, *77*, 185–246.

Jackson, J., and D. McKenzie (1988), The relationship between plate motions and seismic tremors, and the rates of active deformation in the Mediterranean and Middle East, *Geophys. J. R. Astron. Soc.*, *93*, 45–73.

Jackson, J., K. Priestley, M. Allen, and M. Berberian (2002), Active tectonics of the south Caspian Basin, *Geophys. J. Int.*, *148*, 214–245.

Jestin, F., P. Huchon, and J. Gaulier (1994), The Somali plate and the East African rift system: Present-day kinematics, *Geophys. J. Int.*, *116*, 637–654.

Jiménez-Munt, I., and R. Sabadini (2002), The block-like behavior of Anatolia envisaged in the modeled and geodetic strain rates, *Geophys. Res. Lett.*, *29*(20), 1978, doi:10.1029/2002GL015995.

Joffe, S., and Z. Garfunkel (1987), Plate kinematics of the Red Sea–a re-evaluation, *Geophys. J. Int.*, *116*, 637–654.

Kahle, H.-G., M. Concord, Y. Peter, A. Geiger, R. Reilinger, A. Barka, and G. Veis (2000), GPS derived strain rate field within the boundary zones of the Eurasian, African, and Arabian plates, *J. Geophys. Res.*, *105*, 23,353–23,370.

King, R. W., and Y. Bock (2004), Documentation of the MIT GPS analysis software: GAMIT, Mass. Inst. of Technol., Cambridge.

Klinger, Y., J. P. Avouac, N. Abou Karaki, L. Dorbath, D. Bourles, and J. L. Reyes (2000), Slip rate on the Dead Sea transform fault in the northern Araba valley (Jordan), *Geophys. J. Int.*, *142*, 755–768.

Kocyigit, A., and A. Beyhan (1998), A new intra-continental transcurrent structure: The Central Anatolian Fault Zone, Turkey, *Tectonophysics*, *284*, 317–336.

Kozaci, O., J. F. Dolan, R. Finkle, R. D. Hartleb, and M. Gurcan (2005), A 2000-year geologic slip rate for the North Anatolian Fault using cosmogenic CL36 dating, *Eos Trans. AGU*, *86*(52), Fall Meeting Suppl., Abstract G53A-0869.

Le Pichon, X., and J. Angelier (1979), The Hellenic arc and trench system: A key to the neotectonic evolution of the eastern Mediterranean area, *Tectonophysics*, *60*, 1–42.

Le Pichon, X., N. Chamot-Rooke, S. Lallemant, R. Noomen, and G. Veis (1995), Geodetic determination of the kinematics of central Greece with respect to Europe: Implications for eastern Mediterranean tectonics, *J. Geophys. Res.*, *100*, 12,675–12,690.

Le Pichon, X., N. Chamot-Rooke, C. Rangin, and A. M. C. Sengör (2003), The North Anatolian fault in the Sea of Marmara, *J. Geophys. Res.*, *108*(B4), 2179, doi:10.1029/2002JB001862.

Lundgren, P., D. Giardini, and R. Russo (1998), A geodynamic framework for eastern Mediterranean kinematics, *Geophy. Res. Lett.*, *25*, 4007–4010.

Lyberis, N., T. Yurur, J. Chorowicz, E. Kasapoglu, and N. Gundogdu (1992), East Anatolian fault: An oblique collision belt, *Tectonophysics*, *204*, 1–15.

Mahmoud, S., R. Reilinger, S. McClusky, P. Vernant, and A. Tealeb (2005), GPS evidence for northward motion of the Sinai block: Implications for E. Mediterranean tectonics, *Earth Planet. Sci. Lett.*, *238*, 217–224.

Mantovani, E., M. Viti, N. Cenni, and D. Babbucci (2001), Short and long term deformation patterns in the Aegean-Anatolian system: Insights from space-geodetic data (GPS), *Geophys. Res. Lett.*, *28*, 2325–2328.

McCaffrey, R. (2002), Crustal block rotations and plate coupling, in *Plate Boundary Zones*, *Geodyn. Ser.*, vol. 30, edited by S. Stein and J. Freymueller, pp. 101–122, AGU, Washington, D. C.

McClusky, S., et al. (2000), Global Positioning System constraints on plate kinematics and dynamics in the eastern Mediterranean and Caucasus, *J. Geophys. Res.*, *105*, 5695–5719.

McClusky, S., R. Reilinger, S. Mahmoud, D. Ben Sari, and A. Tealeb (2003), GPS constraints on Africa (Nubia) and Arabia plate motions, *Geophys. J. Int.*, *155*, 126–138.

McKenzie, D. P. (1970), Plate tectonics of the Mediterranean region, *Nature*, *226*, 239–243.

McKenzie, D. P. (1972), Active tectonics of the Mediterranean region, *Geophys. J. R. Astron. Soc.*, *30*, 109–185.

McKenzie, D. P. (1978), Active tectonics of the Alpine-Himalayan belt: The Aegean Sea and surrounding regions, *Geophys. J. R. Astron. Soc.*, *55*, 217–254.

McKenzie, D. P., D. Davies, and P. Molnar (1970), Plate tectonics of the Red Sea and East Africa, *Nature*, *226*, 243–248.

McQuarrie, N., J. M. Stock, C. Verdel, and B. P. Wernicke (2003), Cenozoic evolution of Neotethys and implications for the causes of plate motions, *Geophys. Res. Lett.*, *30*(20), 2036, doi:10.1029/2003GL017992.

Meade, B. J., and B. H. Hager (2005), Block models of crustal motion in southern California constrained by GPS measurements, *J. Geophys. Res.*, *110*, B03403, doi:10.1029/2004JB003209.

Meade, B. J., et al. (2002), Estimates of seismic potential in the Marmara region from block models of secular deformation constrained by GPS measurements, *Bull. Seismol. Soc. Am.*, *92*, 208–215.

Meghraoui, M., et al. (2003), Evidence for 830 years of seismic quiescence from paleoseismology, archaeoseismology, and historical seismicity along the Dead Sea fault in Syria, *Earth Planet. Sci. Lett.*, *210*, 35–52.

Meijer, P. T., and M. J. R. Wortel (1997), Present-day dynamics of the Aegean region: A model analysis of the horizontal pattern of stress and deformation, *Tectonics*, *16*, 879–895.

Molnar, P., and P. Tapponier (1975), Cenozoic tectonics of Asia: Effects of continental collision, *Science*, *189*, 419–426.

Niemi, T. M., H. Zhang, M. Atallah, and J. B. J. Harrison (2001), Late Pleistocene and Holocene slip rate of the northern Wadi Araba fault, Dead Sea Transform, Jordan, *J. Seismol.*, *5*, 449–474.

Nyst, M., and W. Thatcher (2004), New constraints on the active tectonic deformation of the Aegean, *J. Geophys. Res.*, *109*, B11406, doi:10.1029/2003JB002830.

Okada, Y. (1985), Surface deformation due to shear and tensile faults in a half-space, *Bull. Seismol. Soc. Am.*, *75*, 1135–1154.

Ozalaybey, S., M. Ergin, M. Aktar, C. Tapirdamaz, F. Bicmen, and A. Yoruk (2002), The 1999 Izmit earthquake sequence in Turkey: Seismological and tectonic aspects, *Bull. Seismol. Soc. Am.*, *92*, 376–386.

Pearce, J. A., et al. (1990), Genesis of collision volcanism in eastern Anatolia, Turkey, *J. Volcanol. Geotherm. Res.*, *44*, 189–229.

Philip, H., A. Cisternas, A. Gviskiani, and A. Gorshkov (1989), The Caucasus: An actual example of the initial stages of continental collision, *Tectonophysics*, *161*, 1–21.

Philip, H., A. Avagyan, A. Karakhanian, J.-F. Ritz, and S. Rabai (2001), Estimating slip rates and recurrence intervals for strong earthquakes along an intercontinental fault: Example of the Pambak-Sevan-Sunik fault (Armenia), *Tectonophysics*, *343*, 205–232.

Provost, A.-S., J. Chery, and R. Hassani (2003), 3D mechanical modeling of the GPS velocity field along the North Anatolian fault, *Earth Planet. Sci. Lett.*, *209*, 361–377.

Ray, J., D. Dong, and Z. Altamimi (2004), IGS reference frames: Status and future improvements, paper presented at IGS 2004 Workshop, Berne, Switzerland, 1 March .

Reilinger, R., and S. McClusky (2001), GPS constraints on block motions and deformations in western Turkey and the Aegean: Implications for earthquake hazards, in *Seismotectonics of the North-western Anatolia-Aegean and Recent Turkish Earthquakes*, edited by T. Taymaz, pp. 14–20, Istanbul Tech. Univ., Istanbul, Turkey.

Reilinger, R., et al. (1997), Global Positioning System measurements of present-day crustal movements in the Arabia-Africa-Eurasia plate collision zone, *J. Geophys. Res.*, *102*, 9983–9999.

Reilinger, R. E., et al. (2000), Coseismic and postseismic fault slip for the 17 August, $M = 7.5$, Izmit, Turkey earthquake, *Science*, *289*, 1519–1524.

Ritz, J.-F., H. Nazari, A. Ghassemi, R. Salamati, A. Shafei, S. Solaymani, and P. Vernant (2006), Active transtension inside central Alborz: A new insight into the northern Iran–southern Caspian geodynamics, *Geology*, in press.

Royden, L. (1993), The tectonic expression of slab pull at continental convergent boundaries, *Tectonics*, *12*, 303–325.

Savage, J. C. (1990), Equivalent strike-slip earthquakes in half-space and lithosphere-asthenosphere Earth models, *J. Geophys. Res.*, *95*, 4873–4879.

Savage, J. C., and W. H. Prescott (1978), Asthenosphere readjustment and the earthquake cycle, *J. Geophys. Res.*, *83*, 3369–3376.

Sella, G. F., T. H. Dixon, and A. Mao (2002), REVEL: A model for Recent plate velocities from space geodesy, *J. Geophys. Res.*, *107*(B4), 2081, doi:10.1029/2000JB000033.

Şengör, A. M. C., and Y. Yilmaz (1981), Tethyan evolution of Turkey: A plate tectonic approach, *Tectonophysics*, *75*, 181–241.

Şengör, A. M. C., N. Gorur, and F. Saroglu (1985), Strike-slip faulting and related basin formation in zones of tectonic escape: Turkey as a case study, in *Strike-Slip Faulting and Basin Formation*, edited by K. T. Biddle and N. Christie-Blick, *Spec. Publ. SEPM Soc. Sediment. Geol.*, *37*, 227–264.

Şengör, A. M. C., S. Özeren, T. Genç, and E. Zor (2003), East Anatolian high plateau as a mantle-supported, north-south shortened domal structure, *Geophys. Res. Lett.*, *30*(24), 8045, doi:10.1029/2003GL017858.

Şengör, A. M. C., O. Tuysuz, C. Imren, M. Sakinc, H. Eyidogan, N. Gorur, X. LePichon, and C. Rangin (2004), The North Anatolian fault: A new look, *Annu. Rev. Earth Planet. Sci.*, *33*, 1–75.

Sonder, L., and P. England (1989), Effects of temperature dependent rheology on large scale continental extension, *J. Geophys. Res.*, *94*, 7603–7619.

Spakman, W. (1991), Delay-time tomography of the upper mantle below Europe, the Mediterranean, and Asia Minor, *Geophys. J. Int.*, *107*, 309–332.

Steckler, M. S., S. Feinstein, B. P. Kohn, L. Lavier, and M. Eyal (1998), Pattern of mantle thinning from subsidence and heat flow measurements in the Gulf of Suez: Evidence for the rotation of Suez and along-strike flow from the Red Sea, *Tectonics*, *17*, 903–920.

Talebian, M., and J. A. Jackson (2002), Offset on the Main Recent fault of NW Iran and implications for the late Cenozoic tectonics of the Arabia-Eurasia collision zone, *Geophys. J. Int.*, *150*, 422–439.

Tapponier, P., A. Y. LeDain, R. Armijo, and P. Cobbold (1982), Propagating extrusion tectonics in Asia: New insights with experiments with plasticine, *Geology*, *10*, 611–616.

Tapponnier, P., X. Zhiqin, F. Roger, B. Meyer, N. Arnaud, G. Wittlinger, and Y. Jingsui (2001), Oblique stepwise rise and growth of the Tibet Plateau, *Science*, *294*, 1671–1677.

Taymaz, T., H. Eyidogan, and J. Jackson (1991), Source parameters of large earthquakes in the east Anatolian fault zone (Turkey), *Geophys. J. Int.*, *106*, 537–550.

ten Veen, J. H., J. M. Woodside, T. A. C. Zitter, J. F. Dumont, J. Mascle, and A. Volkonsaia (2004), Neotectonic evolution of the Anaximander Mountains at the junction of the Hellenic and Cyprus arcs, *Tectonophysics*, *391*, 35–65, doi:10.1016/j.tecto.2004.07.007.

Thatcher, W. (2003), GPS constraints on the kinematics of continental deformation, *Int. Geol. Rev.*, *45*, 191–212.

Trifonov, V. G., A. S. Karakhanian, and A. J. Kozhurin (1994), Major active faults of the collision area between the Arabian and Eurasian plates, paper presented at the Conference on Continental Collision Zone Earthquakes and Seismic Hazard Reduction, IASPEI/IDNDR, Yerevan, Armenia.

Vernant, P., and J. Chery (2006), Low fault friction in Iran implies localized deformation for the Arabia-Eurasia collision zone, *Earth Planet. Sci. Lett.*, in press.

Vernant, P., et al. (2004a), Present-day crustal deformation and plate kinematics in the Middle East constrained by GPS measurements in Iran and northern Oman, *Geophys. J. Int.*, *157*, 381–398.

Vernant, P., et al. (2004b), Deciphering oblique shortening of central Alborz in Iran using geodetic data, *Earth Planet. Sci. Lett.*, *223*, 177–185.

Wdowinski, S., Y. Bock, G. Baer, L. Prawirodirdjo, N. Bechor, S. Naaman, R. Knafo, Y. Forrai, and Y. Melzer (2004), GPS measurements of current crustal movements along the Dead Sea Fault, *J. Geophys. Res.*, *109*, B05403, doi:10.1029/2003JB002640.

Wessel, R., and W. H. F. Smith (1995), New version of the generic mapping tools released, *Eos Trans. AGU*, *76*, 329.

Westaway, R. (1994), Present-day kinematics of the Middle East and eastern Mediterranean, *J. Geophys. Res.*, *94*, 12,071–12,090.

Westaway, R. (1999), Comment on "A new intra-continental transcurrent structure: The Central Anatolian Fault Zone, Turkey," *Tectonophysics*, *314*, 481–496.

Westaway, R. (2004), Kinematic consistency between the Dead Sea fault zone and the neogene and Quaternary left-lateral faulting in SE Turkey, *Tectonophysics*, *391*, 203–238, doi:10.1016/j.tecto.2004.07.014.

Wortel, M. J. R., and W. Spakman (2000), Subduction and slab detachment in the Mediterranean-Carpathian Region, *Science*, *290*, 1910–1917, doi:10.1126/science.290.5498.1910.

Wright, T. J., B. Parsons, P. C. England, and E. J. Fielding (2004), InSAR observations of low slip rates on the major faults of western Tibet, *Science*, *305*, 236–239.

Zor, E., E. Sandvol, C. Gürbüz, N. Türkelli, D. Seber, and M. Barazangi (2003), The crustal structure of the East Anatolian plateau (Turkey) from receiver functions, *Geophys. Res. Lett.*, *30*(24), 8044, doi:10.1029/2003GL018192.

A. Al-Aydrus, Faculty of Science, Sana'a University, Sana'a, Yemen.

R. Al-Ghazzi, Higher Institute of Applied Science and Technology, Damascus, Syria.

A. ArRajehi, King Abdulaziz City for Science and Technology, P.O. Box 6086, Riyadh 11442, Saudi Arabia.

R. Cakmak and S. Ergintav, Turkish National Science Foundation (TUBITAK), Marmara Research Center, Earth and Marine Sciences Research Institute, Gebze 41470, Turkey.

A. Dmitrotsa and S. V. Filikov, Crimea Radio Astronomical Observatory, Simiez, Crimea, Ukraine.

E. Evren, Geophysics Research Group, University of Ulster, Coleraine, Co. Derry, N. Ireland.

F. Gomez, Department of Geological Sciences, University of Missouri–Columbia, Columbia, MO 65211, USA.

I. Guliev and F. Kadirov, Geology Institute, National Academy of Sciences, Az1143 Baku, H. Cavid 29A, Azerbaijan.

T. Guseva and M. Prilepin, Universal Institute of Physics of the Earth, Moscow, Russia.

G. Hahubia and M. Nadariya, Joint Stock Company "Airgeodetic", Tbilisi, Georgia.

G. Karam, Department of Civil Engineering, Lebanese American University, Jbeil, Lebanon.

S. Lawrence, University Navstar Consortium (UNAVCO), Boulder, CO 80301, USA.

S. Mahmoud and K. Sakr, National Research Institute of Astronomy and Geophysics, Helwan, Cairo, Egypt.

S. McClusky, R. Reilinger, and P. Vernant, Department of Earth, Atmospheric, and Planetary Sciences, Massachusetts Institute of Technology, Cambridge, MA 02139, USA. (reilinge@erl.mit.edu)

H. Ozener, Bogazici University, Kandilli Observatory and Earthquake Research Institute, 34680 Cengelkoy, Istanbul, Turkey.

D. Paradissis, Higher Geodesy Laboratory, National Technical University, 9, Heroon Polytechniou Str., GR-15780 Zographou, Athens, Greece.

R. Stepanyan, National Survey for Seismic Protection, Davidashen-Massiv 4, 375054, Yerevan, Republic of Armenia.